APPENDIX C

BINP TASK 3 – DETERMINATION OF ACTUAL MARGINS IN PLANT PIPING

BINP Task 3 – Determination of Actual Margins in Plant Piping

C. 1 Introduction

Traditional plant piping flaw evaluation procedures use an uncoupled stress analysis and flaw evaluation procedure. The stress analysis typically does not include any feature to account for the degradation at the flawed section, it is traditionally performed using a linear elastic analysis, and it usually is done using a response spectrum analysis that provides only peak loads. Traditional flaw evaluation procedures do include plasticity effects, but they generally assume that the peak load obtained from the stress analysis is load-controlled, they ignore low-cycle fatigue during the seismic event as a crack extension mechanism, and use quasi-static material properties. In fact, real piping and real cracks behave in a nonlinear manner. The presence of the crack can influence the behavior of the rest of the piping, sections remote from the crack can yield and absorb some of the seismic energy that could grow the crack, seismic loads are never sustained, cracks can extend by fatigue even for the few load cycles a crack may experience during a seismic event, and the toughness of the materials is affected by dynamic and cyclic loads. Hence, a traditional flaw evaluation analysis may not accurately reflect the ability of the flaw to sustain seismic loads.

Results of analyses and experiments conducted in the IPIRG-1 and IPIRG-2 programs provided a strong indication that flawed plant piping can withstand far greater loads without failure than traditional flaw evaluation methods suggest. Comparing measured experimental moments and calculated moments for the IPIRG-1 pipe-system experiments, the linear-elastic moments were as much as 40 percent higher than the measured moments (Ref. C.1). Thus, the crack driving force is grossly overestimated. For the IPIRG-1 pipe-system experiments, the R6 Revision 3 Option 1 method under-predicted the flaw stress capacity by as much as 88 percent (Ref. C.1). This happened in spite of the fact that the IPIRG-1 flaws were large and none of the pipe remote from the crack experienced plasticity. Analyses done for the U.S. Department of Energy's New Production Reactor program (Refs. C.2 and C.3) suggested that the differences between traditional flaw evaluation procedures and analyses incorporating nonlinear crack behavior support elimination of an instantaneous double-ended pipe break as the system design basis for this particular reactor design. For the case of a 360-degree internal surface flaw 75-percent deep with a 41-percent of the circumference leaking through-wall crack in 406-mm (16-inch) diameter Schedule 40 TP304 stainless steel pipe at 3 SSE seismic loading, nonlinear analysis indicated that the crack remained stable, whereas a traditional LBB flaw evaluation (linear stress analysis and Net-Section-Collapse fracture analysis) suggested that the flaw would fail because the linearly calculated applied moment of 192.6 kN-m (1,705 in-kips) exceeded the calculated flaw capacity of 38.9 kN-m, (344 in-kips) see Figure C.1, by almost a factor of 5. Based on moment, there was a margin in excess of 5 between the traditional LBB analysis and the more realistic nonlinear analysis for the DOE case.

Prior to the BINP program, there had been no systematic effort to determine whether the margins suggested above can be realized in broad classes of real plant piping systems, flaw locations, and loadings. The lack of any significant failures of nuclear power plant piping, such as loss-of-coolant accidents, indicates that margins on piping design and flaw evaluation may be able to be reduced with a consequent reduction in operating costs, and without compromising plant safety. Clearly, flaw nonlinearity, interaction between the crack and the pipe system, plasticity remote from the crack, and the transient nature of seismic loads all could contribute to margins against piping failure that traditional analyses cannot capture. Conversely, low cycle fatigue in a seismic event, which is generally ignored, may reduce margins. For advanced reactor design, more realistic LBB assessments, plant life extension, and more accurate flaw evaluation procedures, the actual margins in plant piping needed to be quantified.

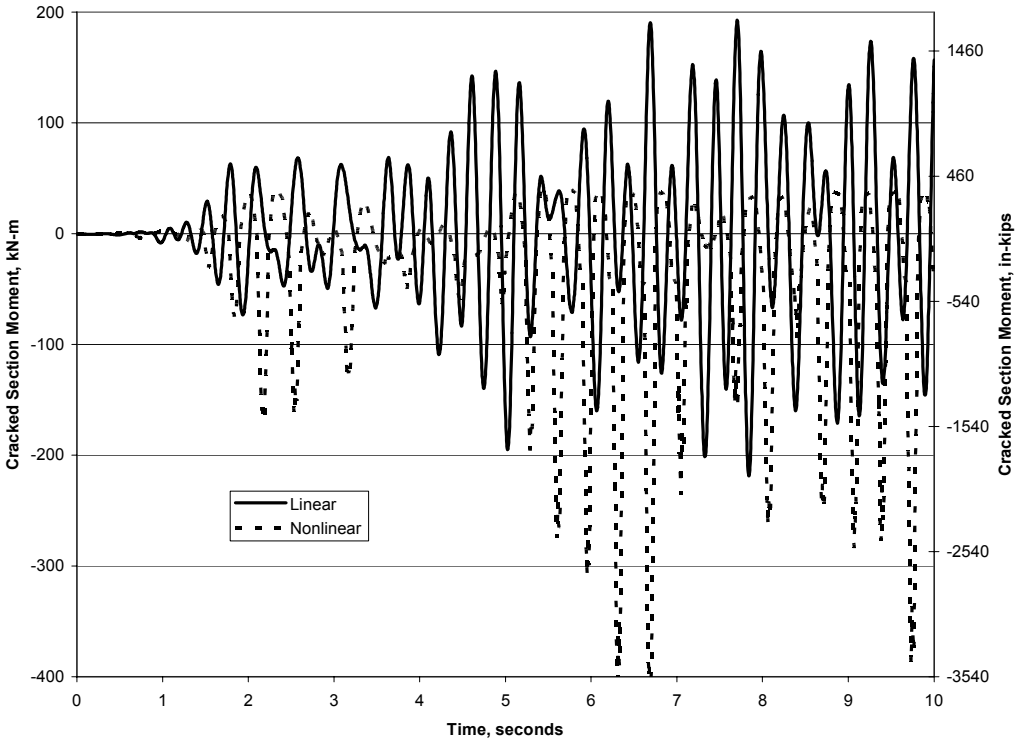

Figure C.1 New Production Reactor moment-time history from both a linear and nonlinear analysis: a large margin exists between these two analyses

C.1.1 Historical Perspective

The original BINP proposal from November 1996 offered an analytical approach to conducting the Actual Margins task. This was to be accomplished by contrasting the results from traditional and advanced nonlinear piping stress analyses on actual plant piping systems submitted for evaluation to Battelle by the TAG. In a subsequent July 1998 meeting of parties interested in participating in the BINP program, it was decided that it would be better if the Actual Margins task was conducted experimentally. Accordingly, a revised statement of work was submitted and accepted wherein two IPIRG cracked pipe system experiments were to be conduced: A single frequency excitation experiment with the high-strength IPIRG pipe replaced by A106 Grade B carbon steel pipe and a second similar experiment using TP304 stainless pipe.

As the BINP program moved forward, there was an evolution of technical interests that, eventually, led to eliminating one of the Actual Margins experiments in favor of some other technical activities. This happened in August 2000. Moving forward with the design of the remaining Actual Margins experiment, it became apparent by January 2001 that it was going to be difficult to conduct a meaningful experiment: The allocated budget was insufficient to conduct an all stainless steel pipe loop experiment and it was virtually impossible to find a carbon steel pipe with a sufficiently low strength to fulfill the task objective of demonstrating margin. In light of this, a decision was made in May 2001 to return to the original concept of doing the Actual Margins task analytically.

C.2 Task Objective and Approach

The objective of the Actual Margins task was to make a systematic assessment of the margin between the load capacity of flawed pipe based on traditional elastic stress analyses of plant pip-

ing and the load capacity based on more realistic nonlinear analyses under seismic loads. The aim was to provide a rational basis for relaxing plant piping stress limitations or simplifying the flaw acceptance criteria in piping design codes.

The work conducted in this task was strictly analytical in nature, although the procedures were experimentally validated in IPIRG-1 (Ref. C.1), IPIRG-2 (Ref. C.4), and a program conducted by Battelle for Argonne National Laboratory (Ref. C.5). Using these previously developed analytical tools, which were supplemented by a few analytical refinements developed during the course of the BINP program, linear and nonlinear analyses were conducted for two classes of problems:

- The IPIRG pipe loop
- Actual plant piping.

The IPIRG pipe loop analyses addressed the question of what we might have learned had the task been done experimentally, while the plant piping analyses addressed real-world practical applications.

Within the two classes of problems, IPIRG pipe loop and plant piping, several different margins were considered:

- The margin between a linear analysis and an analysis that considers nonlinearity due only to a crack in the pipe,
- The margin between a linear analysis and an analysis that considers nonlinearity caused by plasticity remote from the crack, i.e., general yielding in the pipe, and
- The margin between a linear analysis and an analysis that considers the combined nonlinearity of a crack and remote yielding.

The principal output of these analyses was data to determine whether or not the margins from any of the nonlinear analyses are large enough to warrant conducting such a relatively sophisticated analysis for flaw evaluation or LBB applications.

C.3 Preliminary Technical Considerations

Prior to considering the Actual Margins problem, some preliminary technical issues need to be addressed:

- Validation of the ANSYS piping plasticity model
- Moment-rotation of cracks during unloading
- Crack orientation issues.

Although these issues are peripheral to the main focus of the Actual Margins task, they are important elements that enhance the credibility of the results or they are technical details that are required to complete the analyses.

C.3.1 ANSYS Nonlinear Validation

In work previously done at Battelle some years prior to the BINP program, there was some evidence that the ANSYS computer program's pipe elements were too stiff compared with results from the ABAQUS computer program when general plasticity was involved. Because two of the calculated margins of interest from the nonlinear analyses are based on remote yielding, it is important to be sure that the ANSYS program piping elements accurately predicts plastic behavior. Accordingly, a closed-form test problem that would exercise the ANSYS pipe elements in the plastic regime was developed. Identical analyses were performed with ANSYS and ABAQUS and the results compared.

C.3.1.1 Closed-Form Pipe Plasticity Solution

Under the kinematic assumption that plane sections remain plane, radius of curvature, curvature, and strain in a beam bending problem are related to each other by:

$$\frac{1}{\rho} = \kappa = \frac{\varepsilon}{y} \qquad \text{(C.1)}$$

where ρ and y are defined in Figure C.2. This relationship applies independent of the material of the beam, whether or not the beam yields, and what type of constitutive model the beam follows. The stress distribution in the beam is determined by the constitutive model relationship between strain and stress with the strains defined by Equation C.1. The bending moment needed to attain the radius of curvature is simply the integral of the stresses across the cross-section.

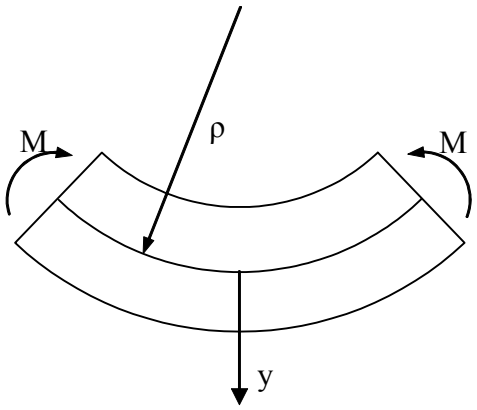

Figure C.2 Plasticity validation bend geometry nomenclature

Using the relationship between curvature and strain for pure bending, a simple closed-form solution for checking finite element beam plasticity formulations can be developed:

1. Pick a cross-sectional shape for the beam
2. Assume a stress-strain constitutive behavior
3. Pick a radius of curvature
4. Calculate the strains throughout the beam cross-section using Equation C.1
5. Using the constitutive model, calculate the stresses in the cross-section
6. Integrate the calculated stresses to find the theoretical moment
7. Integrate the calculated stresses to find the axial force
8. Calculate the theoretical end deflection of the cantilever beam of length as:

$$\theta = \frac{2\ l_0}{\rho} \qquad \text{(C.2)}$$

$$y = \rho(1 - \cos\frac{\theta}{2}) \qquad \text{(C.3)}$$

9. Build a finite element model of the cantilever beam
10. Apply the calculated moment to the finite element model
11. Compare the finite element stresses and strains at various locations in the cross-section to the corresponding theoretical values
12. Compare the theoretical and finite element end deflections.

For the case of bending plus tension, the procedure is altered slightly:

1. An initial axial strain is assumed, ε_0
2. The "stretch" of the beam is found from the definition of axial strain

$$\Delta l = l_o \varepsilon_0 \qquad \text{(C.4)}$$

3. The axial strain is added to the bending strain, the beam elongation is added to the beam length, and the solution proceeds as above.

C.3.1.2 Closed-Form Solution Details

Hutchinson's stress-strain relationship (Ref. C.6), which is represented by the two-segment curve defined in Equations C.5a and C.5b, was used as the constitutive relationship to generate the closed-form solutions:

$$\sigma = E\varepsilon \quad , \quad \varepsilon \le \varepsilon_o \qquad \text{(C.5a)}$$

$$\sigma = \sigma_o \left[\frac{n\varepsilon}{\varepsilon_o} + 1 - n \right]^{\frac{1}{n}} \quad , \quad \varepsilon > \varepsilon_o \qquad \text{(C.5b)}$$

where

ε = strain, in/in
σ = stress, psi
E = Young's modulus, psi
σ_o = stress at proportional limit, psi

ε_o = strain at proportional limit, in/in

$= E / \varepsilon_0$

n = dimensionless exponent greater than 1.0

Inverting this relationship,

$$\varepsilon = \frac{\sigma}{E} \qquad , \varepsilon \le \varepsilon_0 \qquad \text{(C.6a)}$$

$$\varepsilon = \frac{\sigma_0}{E}\left[\frac{1}{n}\left(\frac{\sigma}{\sigma_0}\right)^n + 1 - \frac{1}{n}\right] \quad , \varepsilon > \varepsilon_0 \qquad \text{(C.6b)}$$

With reference to Figure C.3 and under the plane sections remain plane during bending assumption, the strain at any point in a pipe cross-section can be found:

$$\varepsilon = \frac{y}{\rho} + \varepsilon_t = \frac{r\sin\theta}{\rho} + \varepsilon_t \qquad \text{(C.7)}$$

The moment is given by

$$M = \int_A \sigma y \, dA \qquad \text{(C.8)}$$

$$= 2\int_{-\pi/2}^{\pi/2}\int_a^b \sigma(r,\theta,\rho)\, r^2 \sin\theta \; dr \; d\theta \qquad \text{(C.9a)}$$

or, equivalently,

$$M = \int_0^{2\pi}\int_{\varepsilon_b}^{\varepsilon_a} \frac{\sigma\varepsilon^2\rho^3}{(\sin\theta)^3}\, d\varepsilon \; d\theta \qquad \text{(C.9b)}$$

The axial force is given by

$$F = \int_A \sigma \; dA \qquad \text{(C.10)}$$

$$= 2\int_{-\pi/2}^{\pi/2}\int_a^b \sigma(r,\theta,\rho)\, r \; dr \; d\theta \qquad \text{(C.11a)}$$

or, equivalently,

$$M = \int_0^{2\pi}\int_{\varepsilon_b}^{\varepsilon_a} \frac{\sigma\varepsilon\rho^2}{(\sin\theta)^2}\, d\varepsilon \; d\theta \qquad \text{(C.11b)}$$

The integrals in Equations C.9 and C.11 are not amenable to a closed-from solution. Accordingly, Guass quadrature was used to approximate the integrals. For a single integral,

$$\int_a^b f(y)dy \cong \left(\frac{b-a}{2}\right)\sum_{i=1}^{n} w_i f(y_i) \qquad \text{(C.12a)}$$

$$y_i = \left(\frac{b-a}{2}\right)x_i + \left(\frac{b+a}{2}\right) \qquad \text{(C.12b)}$$

where x_i, w_i are tabulated abscissas and weight factors that can be found in reference texts on numerical methods. For double integrals, as shown in Equations C.9 and C.11, two successive applications of Equation C.12 are required.

C.3.1.2 Plasticity Validation Results

The validation analysis was conducted using the parameters shown in Table C.1. Tables C.2 and C.4 list the theoretical values for the pure bending and bending plus tension load cases, respectively, and Tables C.3 and C.5 list deviations from these theoretical values for the various finite element analyses. Values for listed strains are at theta = 90 degrees at the mid-thickness of the pipe wall.

The ANSYS finite element model solution consisted of 20 PIPE20 elements fixed at one end with a moment applied to the free end. The moment was varied to produce different curvatures in the pipe and, accordingly, different strains. An axial force was applied to the free end of the cantilevered pipe followed by various moments to produce the bending with axial load results. Multi-linear isotropic hardening

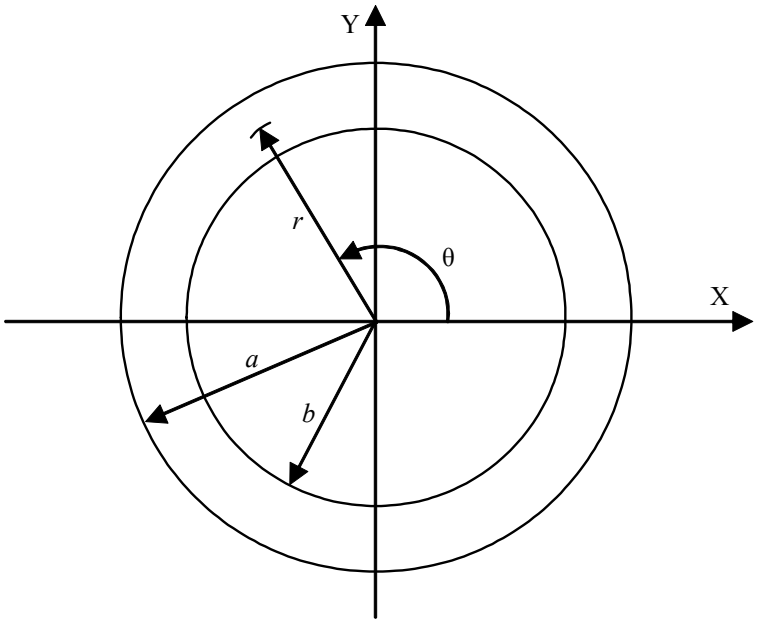

Figure C.3 Plasticity validation pipe cross-section nomenclature

Table C.1 Plasticity validation analysis parameters

Constant	Value
a	203.2 mm (8.00 inch)
b	172.2 mm (6.781 inch)
E	206.85 GPa ($30x10^6$ psi)
σ_o	206.85 MPa ($30x10^3$ psi)
ε_o	0.001 mm/mm (inch/inch)
n	7.0
ε_t	0.0006 mm/mm (inch/inch)
l_0	508 mm (20 inch)

Table C.2 Plasticity validation theoretical values for pure bending

Radius of Curvature, m (in)	Moment, kN-m (in-kips)	Strain, mm/mm (in/in)	Stress, MPa (psi)	Deflection, mm (inch)
177.80 (7000)	750.835 (6645.731)	0.001056	216.825 (31447)	0.73 (0.029)
170.18 (6700)	780.535 (6908.615)	0.001103	223.539 (32420)	0.76 (0.030)
165.10 (6500)	800.470 (7085.059)	0.001137	227.706 (33025)	0.78 (0.031)
152.40 (6000)	850.358 (7526.621)	0.001232	237.392 (34430)	0.85 (0.033)
139.70 (5500)	900.226 (7968.008)	0.001344	246.429 (35740)	0.92 (0.036)
132.08 (5200)	930.199 (8233.309)	0.001421	251.689 (36503)	0.98 (0.038)
127.00 (5000)	950.244 (8410.726)	0.001478	255.165 (37007)	1.02 (0.040)
114.30 (4500)	1000.768 (8857.920)	0.001642	263.864 (38269)	1.13 (0.044)
101.60 (4000)	1052.319 (9314.210)	0.001848	272.766 (39560)	1.27 (0.050)
88.90 (3500)	1105.644 (9786.189)	0.002112	282.129 (40918)	1.45 (0.057)
76.20 (3000)	1161.842 (10283.604)	0.002464	292.274 (42389)	1.69 (0.067)
63.50 (2500)	1222.643 (10821.764)	0.002956	303.660 (44041)	2.03 (0.080)

Table C.3 Plasticity validation deviation from theoretical values for pure bending

Radius of Curvature, m (in)	Strain Error, %			Stress, %			Displacement, %		
		ABAQUS			ABAQUS			ABAQUS	
	ANSYS	PIPE31	ELBOW31	ANSYS	PIPE31	ELBOW31	ANSYS	PIPE31	ELBOW31
177.80 (7000)	0.74	2.01	1.25	0.56	-0.68	-1.09	0.74	2.01	1.28
170.18 (6700)	0.97	2.70	1.84	0.62	-1.07	-1.51	0.97	2.69	1.87
165.10 (6500)	1.10	2.97	2.23	0.64	-1.22	-1.60	1.10	2.97	2.26
152.40 (6000)	0.88	2.91	3.14	0.41	-1.42	-1.33	0.88	2.91	3.17
139.70 (5500)	-0.04	1.71	3.85	-0.01	-1.56	-0.61	-0.04	1.71	3.89
132.08 (5200)	-0.94	0.89	3.87	-0.34	-1.44	-0.15	-0.94	0.89	3.90
127.00 (5000)	-1.66	1.20	3.64	-0.57	-0.90	0.13	-1.66	1.21	3.68
114.30 (4500)	-2.30	1.39	2.43	-0.68	0.42	0.84	-2.30	1.39	2.48
101.60 (4000)	-1.74	0.60	0.78	-0.45	1.65	1.71	-1.74	0.60	0.83
88.90 (3500)	0.43	-1.28	-1.71	0.11	2.77	2.58	0.43	-1.28	-1.66
76.20 (3000)	3.52	-4.37	-5.58	0.76	3.74	3.25	3.52	-4.37	-5.52
63.50 (2500)	7.54	-8.82	-10.98	1.46	4.52	3.68	7.54	-8.82	-10.93

Table C.4 Plasticity validation theoretical values for tension plus bending

Radius of Curvature, m (in)	Moment, kN-m (in-kips)	Tension, N (lb)	Strain, mm/mm (in/in)	Stress, MPa (psi)	Deflection, mm (inch)
177.80 (7000)	647.414 (5730.342)	3902 (877168)	0.001656	264.505 (38362)	0.73 (0.029)
170.18 (6700)	669.373 (5924.700)	3829 (860793)	0.001703	266.687 (38678)	0.76 (0.030)
165.10 (6500)	684.982 (6062.857)	3776 (848775)	0.001737	268.190 (38896)	0.78 (0.031)
152.40 (6000)	727.946 (6443.136)	3622 (814195)	0.001832	272.137 (39469)	0.85 (0.033)
139.70 (5500)	777.730 (6883.781)	3432 (771628)	0.001944	276.399 (40087)	0.92 (0.036)
132.08 (5200)	811.668 (7184.170)	3297 (741241)	0.002021	279.133 (40483)	0.98 (0.039)
127.00 (5000)	836.317 (7402.346)	3196 (718537)	0.002078	281.041 (40760)	1.02 (0.040)
114.30 (4500)	905.097 (8011.129)	2904 (652899)	0.002242	286.154 (41502)	1.13 (0.044)
101.60 (4000)	978.159 (8657.807)	2586 (581437)	0.002448	291.859 (42329)	1.27 (0.050)
88.90 (3500)	1049.926 (9293.023)	2276 (511581)	0.002712	298.332 (43268)	1.45 (0.057)
76.20 (3000)	1121.281 (9924.594)	1972 (443418)	0.003064	305.830 (44355)	1.70 (0.067)
63.50 (2500)	1194.443 (10572.160)	1673 (376048)	0.003556	314.764 (45651)	2.03 (0.080)

Table C.5 Plasticity validation deviation from theoretical values for tension plus bending

Radius of Curvature, m (in)	Strain Error, %			Stress, %			Displacement, %		
		ABAQUS			ABAQUS			ABAQUS	
	ANSYS	PIPE31	ELBOW31	ANSYS	PIPE31	ELBOW31	ANSYS	PIPE31	ELBOW31
177.80 (7000)	0.66	4.70	3.26	0.19	0.77	0.15	0.62	4.39	2.65
170.18 (6700)	0.41	4.51	3.03	0.12	0.99	0.35	0.41	4.14	2.35
165.10 (6500)	0.75	4.36	2.88	0.38	1.14	0.50	0.68	3.94	2.14
152.40 (6000)	0.91	3.86	2.42	0.24	1.54	0.90	0.81	3.38	1.60
139.70 (5500)	0.99	3.19	1.86	0.25	1.98	1.36	0.86	2.70	1.00
132.08 (5200)	1.46	2.70	1.44	0.36	2.27	1.67	1.25	2.22	0.59
127.00 (5000)	1.85	2.32	1.13	0.44	2.47	1.88	1.58	1.89	0.29
114.30 (4500)	2.04	1.13	0.10	0.46	2.97	2.44	1.74	0.77	-0.60
101.60 (4000)	2.32	0.00	-1.43	0.53	3.75	3.08	2.15	0.17	-1.76
88.90 (3500)	2.88	-2.61	-3.84	0.60	4.20	3.65	2.28	-2.55	-3.90
76.20 (3000)	1.30	-6.94	-7.28	0.26	4.26	4.16	0.06	-7.53	-7.14
63.50 (2500)	3.15	-11.83	-12.19	-0.84	4.61	4.39	2.81	-11.89	-12.22

(ANSYS MISO model) was used to model the stress-strain behavior using 86 points to define the curve. Default convergence criteria were used. The analyses were conducted with ANSYS/ED 5.7 running on a desktop PC.

The ABAQUS solution used PIPE31 or ELBOW31 elements. Again, 20 elements were used along the length of a cantilever beam. The same 86 points were used to define the stress-strain curve, and default convergence criteria were used. ABAQUS 5.8 running on a Sun UltraSparc was used to generate the solutions.

All of the models used in the plasticity evaluation are listed in section C.6.1.

C.3.1.3 Plasticity Validation Summary

The results of the analyses show that both ANSYS and ABAQUS give results in reasonably good agreement with the theoretical solutions. General observations, based on the cases considered include: 1) the finite element solutions are within about 10 percent of the theoretical solutions, 2) both programs have some solutions that are above and some solutions that are below the theoretical values, depending on the load level, 3) higher loads tend to have greater absolute errors, 4) the ANSYS solution for combined tension and bending is better than the pure bending solution while the opposite is true for the ABAQUS solutions, and 5) the largest absolute errors occur with ABAQUS ELBOW31 elements.

In terms of the Actual Margins task, the results of this study indicate that the ANSYS pipe plasticity model is perfectly acceptable for the analyses that consider plasticity remote from the crack.

C.3.2 Moment-Rotation Behavior of Cracks During Unloading

The behavior of a crack undergoing unloading needs to be carefully considered in a nonlinear finite element analysis. Crack behavior is inherently asymmetric—pressure reduces the moment carrying capacity during loading, but it certainly does not promote compressive yielding. Because the nonlinear crack will usually follow some sort of standard plasticity hardening rule and these rules are generally symmetric in their behavior, crack models based on elements that use these hardening rules may not unload correctly after yielding unless special precautions are taken.

An approach to crack unloading, developed during the BINP program is presented in the following discussion. Although the work as presented is focused on circumferential surface cracks, extension to the case of circumferential through-wall and axial cracks is not difficult.

C.3.2.1 Moment-Rotation General Considerations

Nonlinear crack behavior of a circumferential crack in a finite element analyses can be characterized as crack moment versus crack rotation and can be implemented as a set of three elastic-perfectly plastic springs in series, see Figure C.4. Implicit with the elastic-plastic spring formulation is the assumption of kinematic hardening, i.e., yielding in the compressive direction occurs at $2\sigma_y$ below a plastic unloading point, Figure C.5. This is equivalent to saying that the compressive moment-rotation response is the mirror image of the tension moment-rotation response. Furthermore, because the nonlinear behavior of the crack is modeled only as moment-rotation, effects such as axial loading, which affects the state of stress at the crack tip, must be “built into” the moment-rotation curve. That is, a crack with pressure and moment loading will have an apparently lower moment-rotation resistance than a crack with moment only loading, Figure C.6.

For cases where crack loading is always tensile and reverse yielding never occurs, a kinematic hardening model using the pressure-corrected case is perfectly suitable. However, if significant reverse loading is expected, i.e., seismic loading, compressive yielding will occur far too early if a pressure-corrected moment rotation curve is used as the basis of the crack model. Basically, because the pressure-corrected moment-rotation curve is the mirror image of the tensile moment-rotation curve, it is as if the

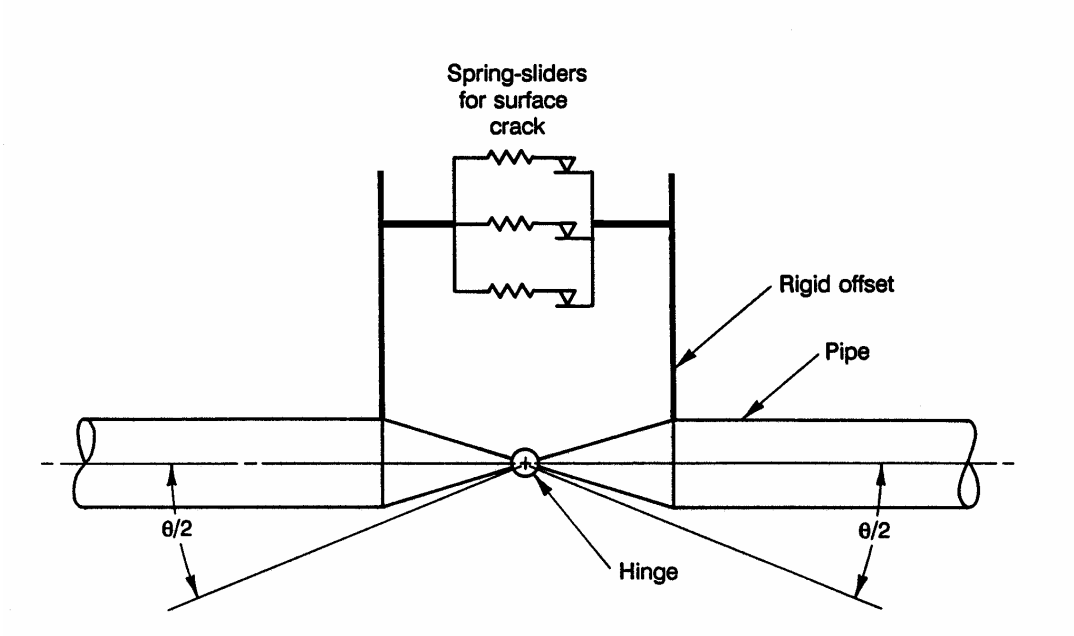

Figure C.4 Spring-slider model for a surface crack (or a through-wall crack)

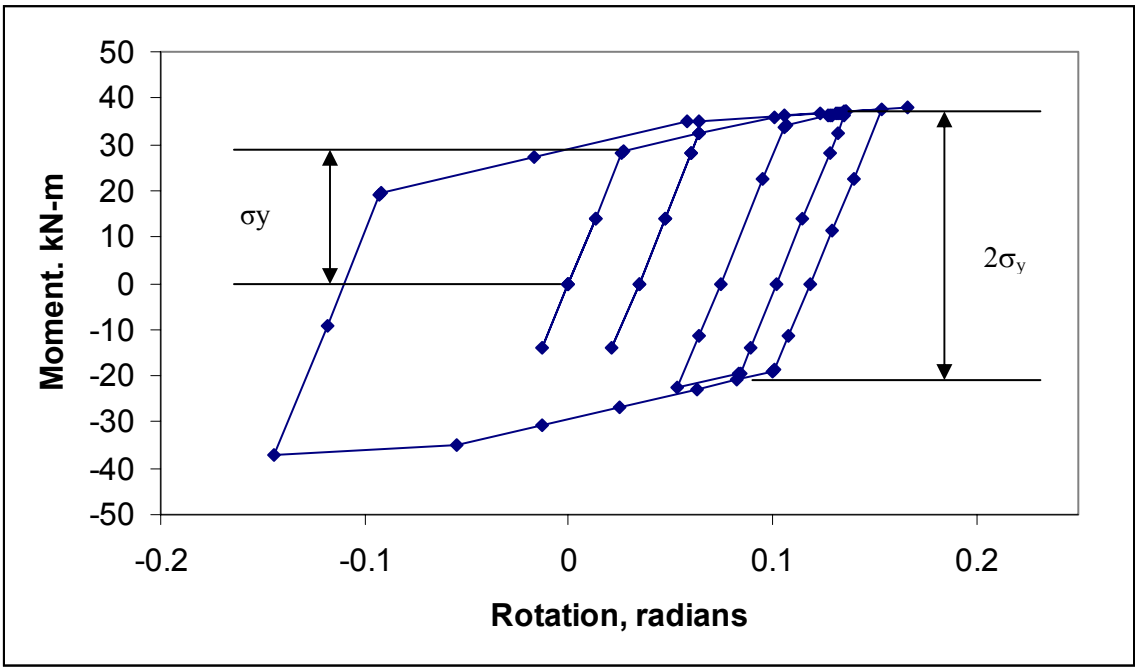

Figure C.5 Kinematic hardening assumption under unloading conditions

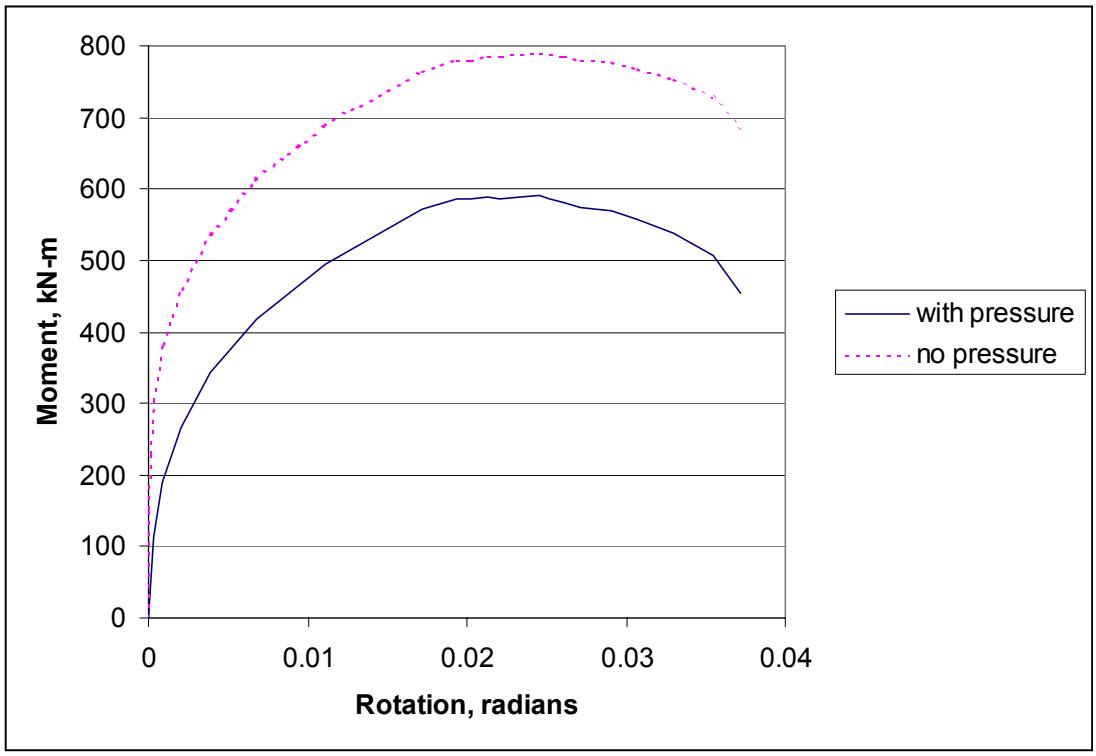

Figure C.6 The effect of pressure on crack moment-rotation behavior (BINP Task 2 flaw, A8ii-20 dynamic monotonic J-resistance)

stress at the crack tip caused by pressure changes sign when the crack is unloaded: A totally inappropriate response. The crack should unload elastically much further before it yields in compression, Figure C.7. This is quite important for an LBB analysis or a flaw evaluation analysis where one is trying to find margin, because it is the unloading and subsequent compressive yielding that takes energy away from driving the crack.

C.3.2.2 Model for Crack Unloading

Any new modeling approach for circumferential cracks loaded with pressure and bending to better define the compressive loading behavior needs to include the following:

- Tensile loading failure based on pressure plus bending,
- Consistency with kinematic hardening rules, i.e., $2\sigma_y$ yielding behavior, and
- Compressive loading must account for the pressure effect.

Taken as a whole, these conditions imply that the moment-rotation response of the crack must be asymmetric, i.e., compression is not a mirror image of tension. The last two conditions imply that compressive yielding in moment-rotation coordinates must occur at twice the tensile yield moment (including the pressure effect) plus twice the pressure-induced moment effect. Figure C.7 provides a pictorial representation of the desired behavior.

Implementation of asymmetry in the moment-rotation response in the finite element model would, in general, require a special constitutive model or a special element that is not likely in a standard finite element library. The desired response, however, can be achieved with kinematic hardening elements as follows:

1. Define the expected tensile crack moment-rotation behavior using a J-estimation scheme analysis that includes pressure,

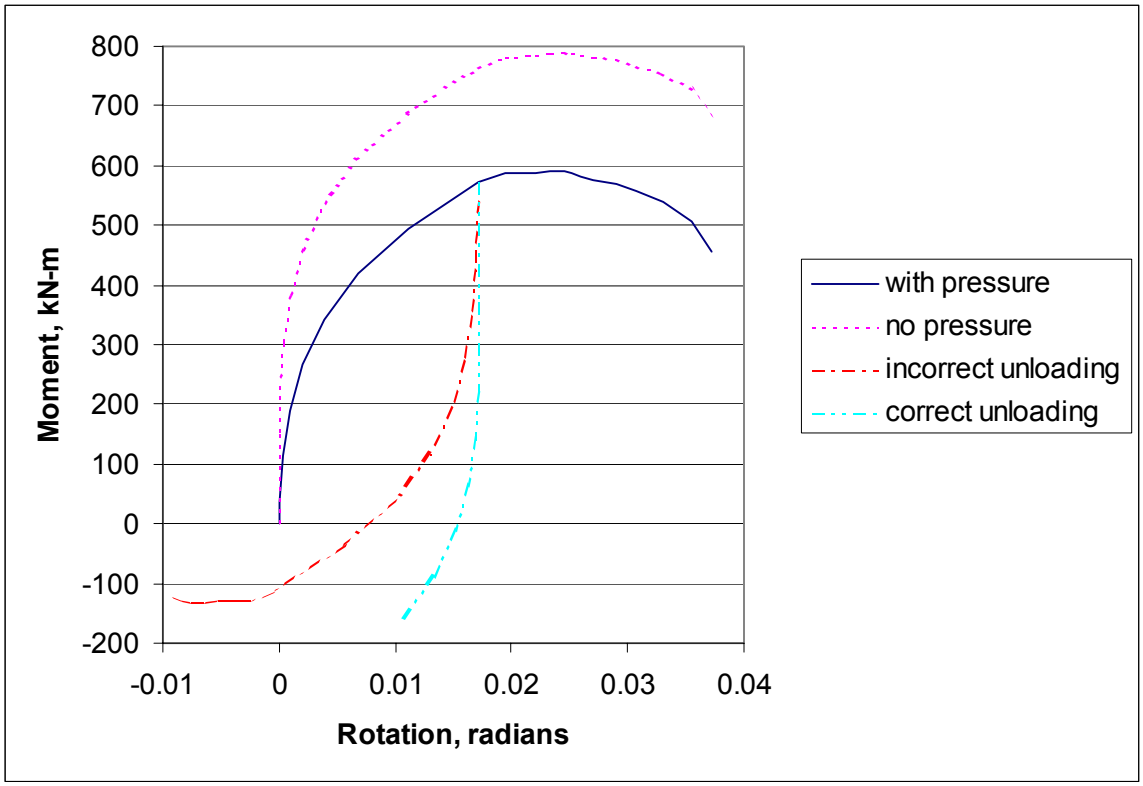

Figure C.7 Crack unloading behavior

2. Define the pressure contribution to the tensile failure by running a J-estimation scheme analysis identical to the first one but without pressure,
3. Use the data from the second analysis to define the "springs" and "sliders" for the nonlinear crack model,
4. Apply + and - crack opening moments at the two nodes of the spring-sliders equal to the moment difference between the results from Step 1 and Step 2, and
5. Conduct the analysis as usual.

The net effect of this process is to make the crack moment-rotation response appear asymmetric as far as tensile and compressive yielding of the crack is concerned. However, as far as the pipe system is concerned the correct crack response is modeled:

- The stresses in the pipe will be calculated correctly because the moments applied in Step 4 sum to zero.
- The incremental tensile moment that the crack can stand will be correct because the moments applied in Step 4 make up the difference between the moments the spring sliders in the model will permit and the real failure moment calculated in Step 1.

One does have to be careful about recovering and reporting moments at the crack because the apparent moment in the spring sliders will be too large by the offset moment.

C.3.2.3 Crack Unloading Model Validation

To provide some level of comfort that the proposed crack unloading model is rational, an analysis of the IPIRG-2 Experiment 1-1 (Ref. C.4) surface crack experiment was conducted to see how well the analysis compares with an experiment. Figures C.8 and C.9 show the measured pipe response from the experiment up to surface-crack penetration.

The result of the cracked pipe analysis is driven by the input moment-rotation response, which, in turn, is determined by the J-estimation scheme crack growth analysis. To bound the

expected behavior, analyses were conducted using moment-rotation curves developed from J-R curves for R = -0.3 and R = 1.0, because the stress ratio for the experiment is about R = -0.6. The predicted moment-rotation behavior for the IPIRG-2 1-1 experiment, generated using the SC.TNP1 analysis in NRCPIPES Version 3.0, is shown in Figure C.10. For these curves, the equivalent crack length (measured crack area divided by the measured maximum depth) was used. There are significant differences between these curves because at R = -0.3 there is very little degradation from the monotonic J-R curve case, whereas at R = -1.0 the J-R curve, and hence moment-rotation is significantly affected by crack closure.

Using the design seismic forcing function for IPIRG-2 Experiment 1-1 (there is virtually no difference between the designed function and the experimentally measured actuator response), ANSYS nonlinear-spring analyses were conducted to the point of maximum load, i.e., presumed surface-crack penetration, using the new compressive unloading behavior model. Figures C.11 through C.14 show the results of the "bounding" analyses. For reference, Figures C.15 and C.16 show the results of the IPIRG-2 1-1 pretest analysis that used the mirror image of the bending plus tension moment-rotation response in the compressive regime.

Comparing Figures C.8, C.11, C.13 and C.15, qualitatively, the new analyses are much closer to the experiment than the "old" analysis in two regards: 1) the new analyses do not show the severe crack closures that the old analysis did, and 2) the new analyses show evidence of the large monotonic load cycle that the old analysis did not predict. Quantitatively, the new R = -0.3 and R = -1.0 analyses bracket the experimentally observed R = -0.6 failure moment, whereas the old analysis is low, although there is a good reason for this—the old analysis was a pretest prediction that used the best pretest estimate of the flaw size, whereas the new analyses used the measured flaw size. Quantitatively, it is also important to note that the rotations in the new analyses are very much larger than the experimentally observed rotations. This is a J-estimation scheme problem—the ANSYS nonlinear spring analysis is only as good as the input from the J-estimation scheme. As a final observation, in the experiment, surface-crack penetration occurred long after maximum moment. Within the bounds of the ANSYS nonlinear spring analysis, this just cannot be predicted because surface-crack penetration is defined to happen at maximum moment. From an experimental perspective, what this implies is that there was either cyclic or fatigue damage that contributed to the eventual failure.

C3.2.4 Crack Unloading Model Summary

The new technique for modeling a crack as it unloads accounts for the expected asymmetric behavior of a crack using a simple hardening rule-based plasticity model. Although there is not a way to rigorously prove that the model is correct because there is not enough quality experimental data available, from a heuristic perspective, it makes sense to use such a model for all plant piping analyses. The issue of which J-R curve to use, R = 0, or R = -?, will always be a question, but the basic mechanics of defining the springs is not in question.

C.3.3 Crack Orientation

In a general finite element analysis of plant piping, some arbitrary global reference coordinate system is used to define the location of all piping system features. Except for a few fortuitous instances, the global coordinate system rarely is aligned orthogonally with the orientation of cracks that may be hypothesized in the piping. Thus, the job of putting nonlinear springs with constraint equations to model cracks at arbitrary orientations becomes a bit of a challenge.

A brute-force approach to putting a spring or constraint at an arbitrary orientation would involve specification of the orientation in terms of Euler angles and applying a series of coordinate transformations to spring stiffnesses and constraint equations. Fortunately, most finite element programs have a far more elegant and simple way to define orientations: Local coordinate systems. The notion of using local coordinates is not revolutionary or new, but it is

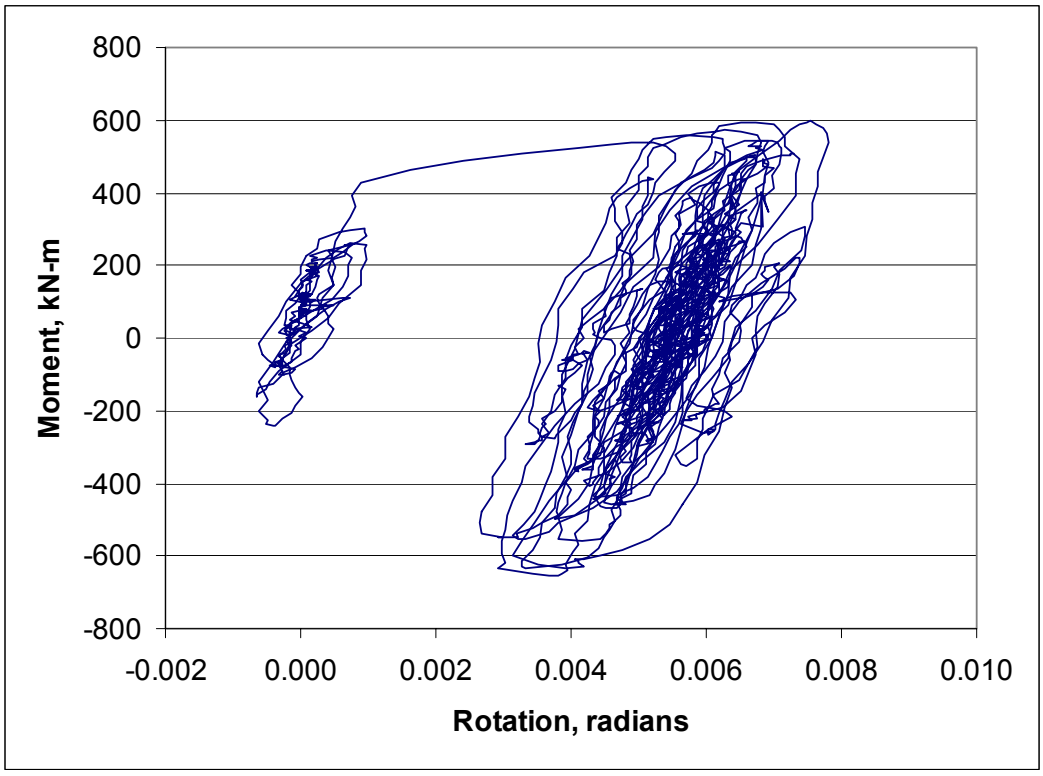

Figure C.8 IPIRG-2 Experiment 1-1 cracked-section moment-rotation response

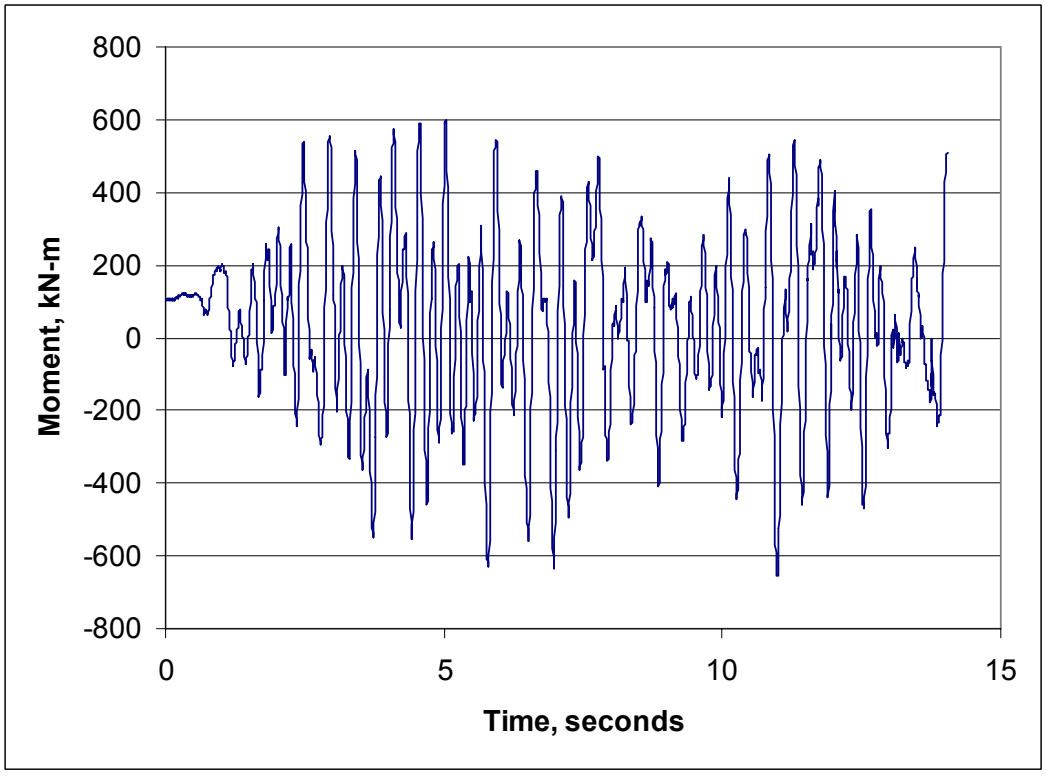

Figure C.9 IPIRG-2 Experiment 1-1 cracked-section moment-time history

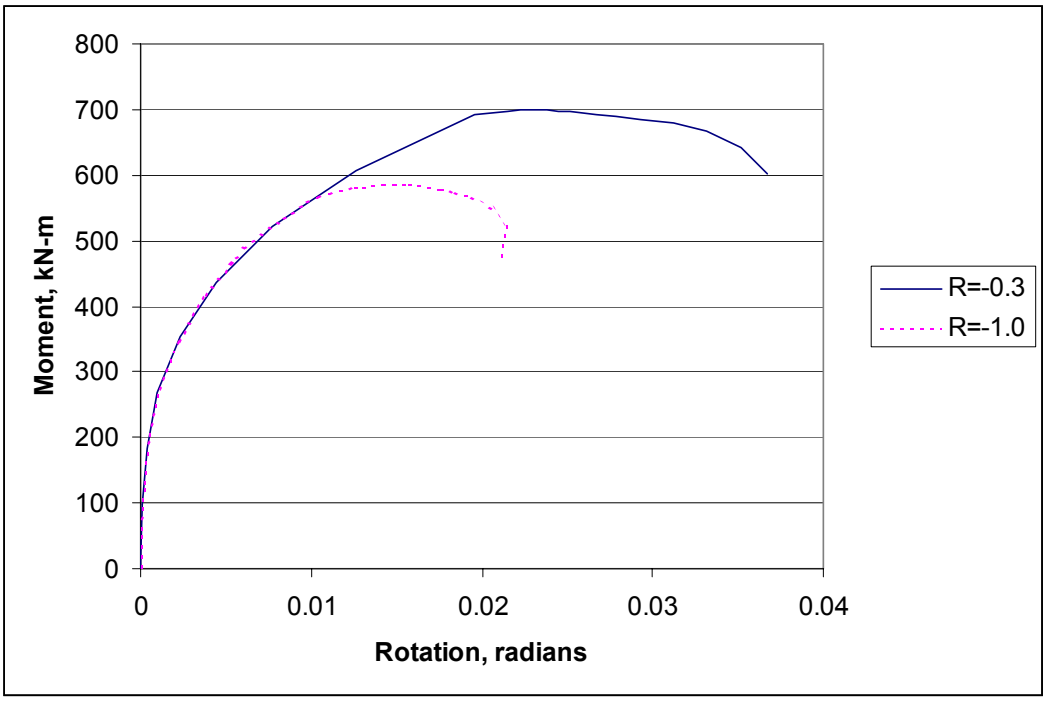

Figure C.10 IPIRG-2 Experiment 1-1 predicted cracked-section upper envelop moment-rotation from the SC.TNP1 J-estimation scheme

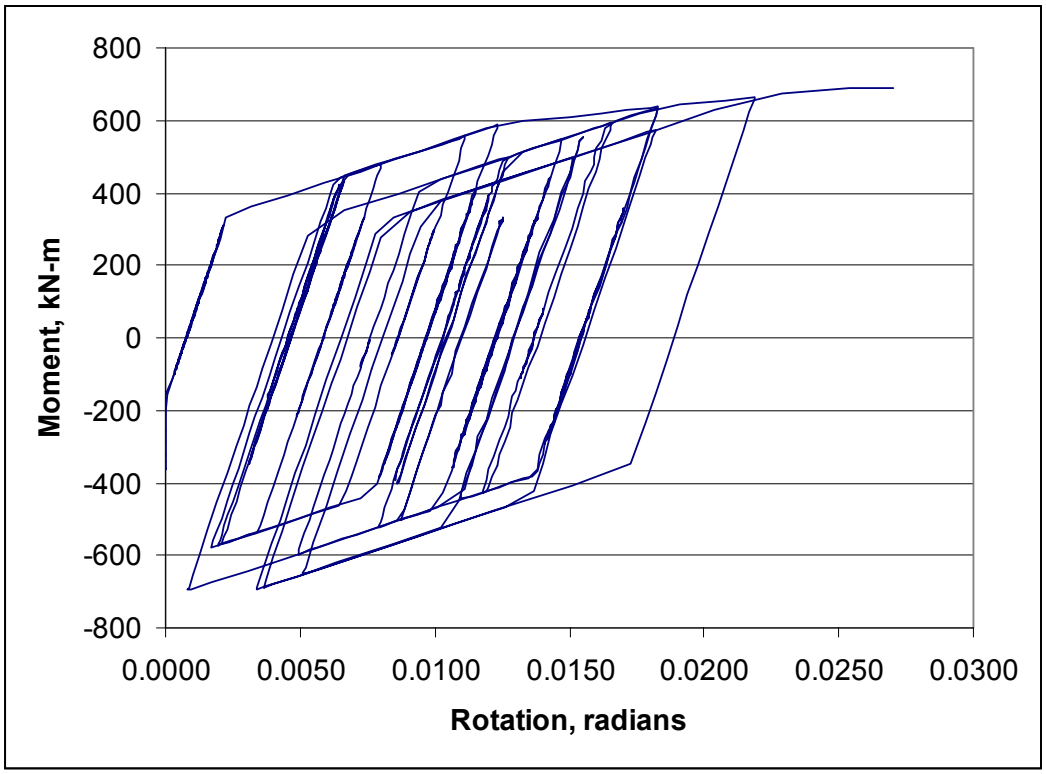

Figure C.11 Predicted IPIRG-2 Experiment 1-1 moment-rotation history using the dynamic R=-0.3 J-R curve with the new asymmetric moment-rotation model

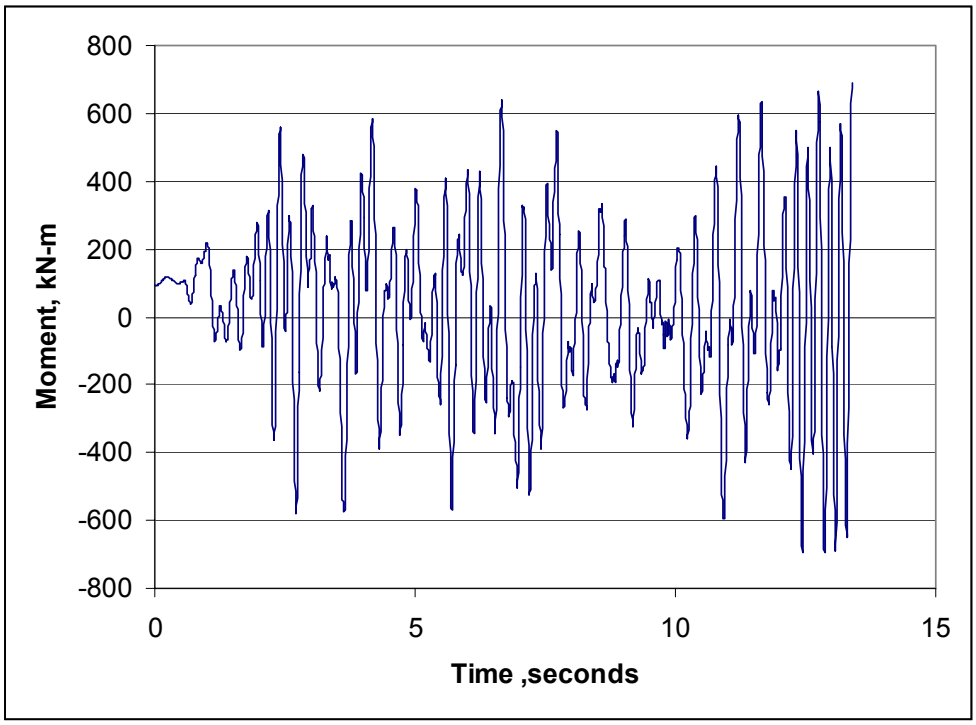

Figure C.12 Predicted IPIRG-2 Experiment 1-1 moment-time history with the dynamic R=-0.3 J-R curve with the new asymmetric moment-rotation model

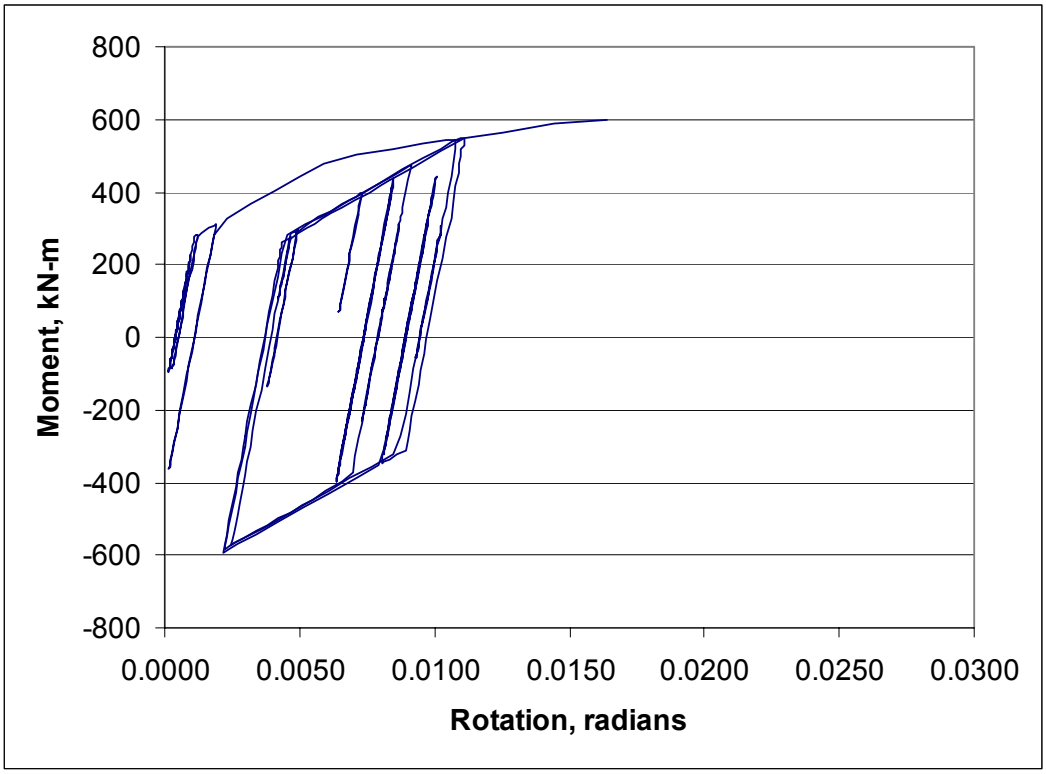

Figure C.13 Predicted IPIRG-2 Experiment 1-1 moment-time history with the dynamic R=-1.0 J-R curve with the new asymmetric moment-rotation model

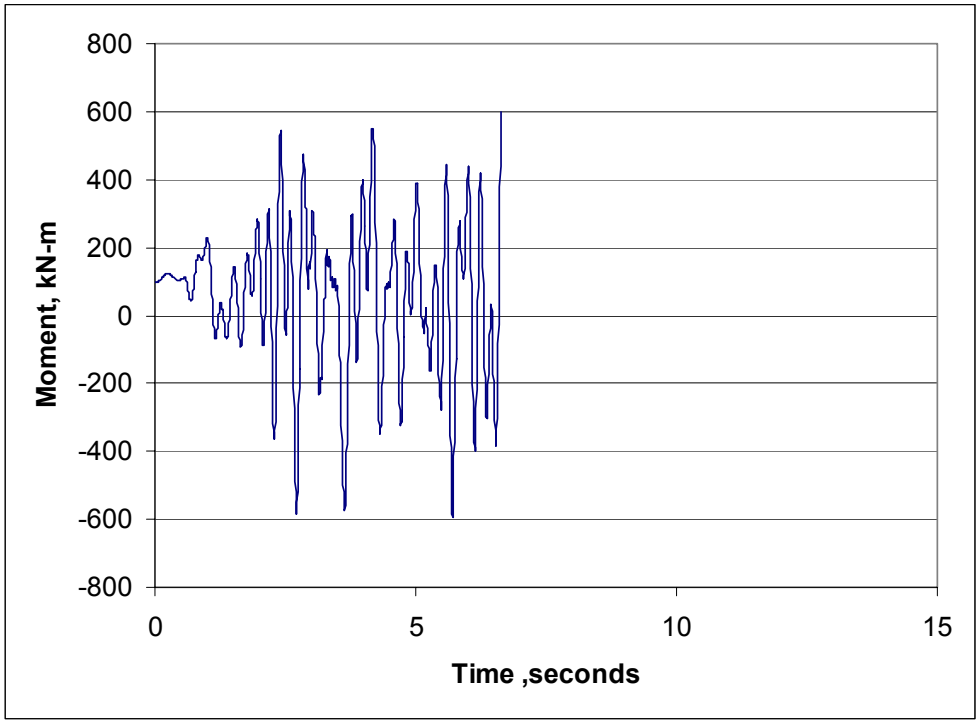

Figure C.14 Predicted IPIRG-2 Experiment 1-1 moment-time history with the dynamic R=-1.0 J-R curve with the new asymmetric moment-rotation model

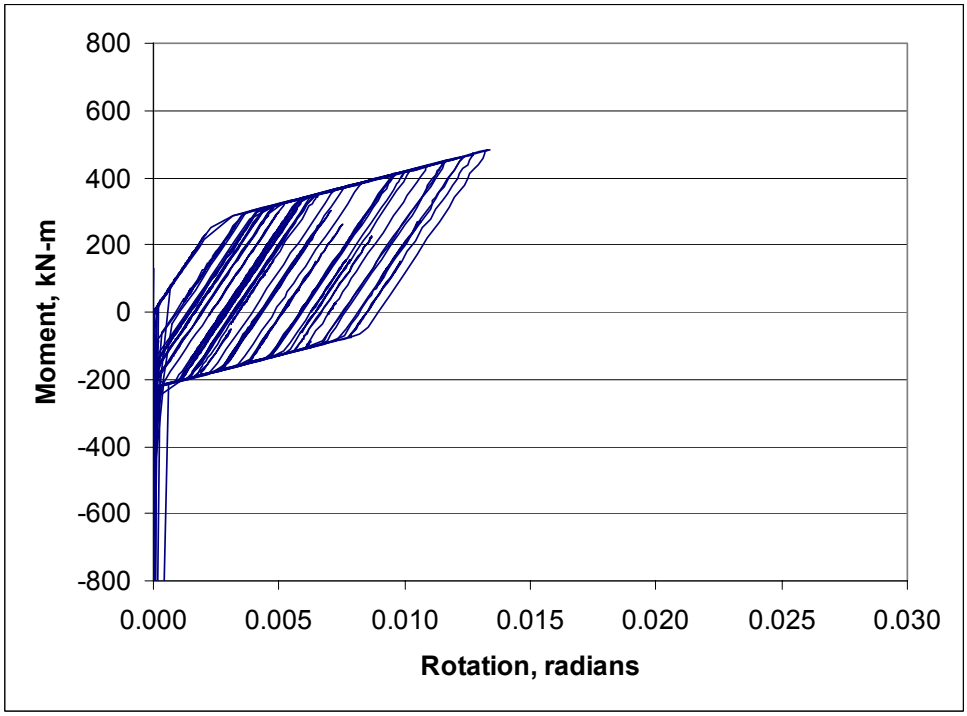

Figure C.15 Old (1993) IPIRG-2 Experiment 1-1 pretest design analysis moment-rotation history results

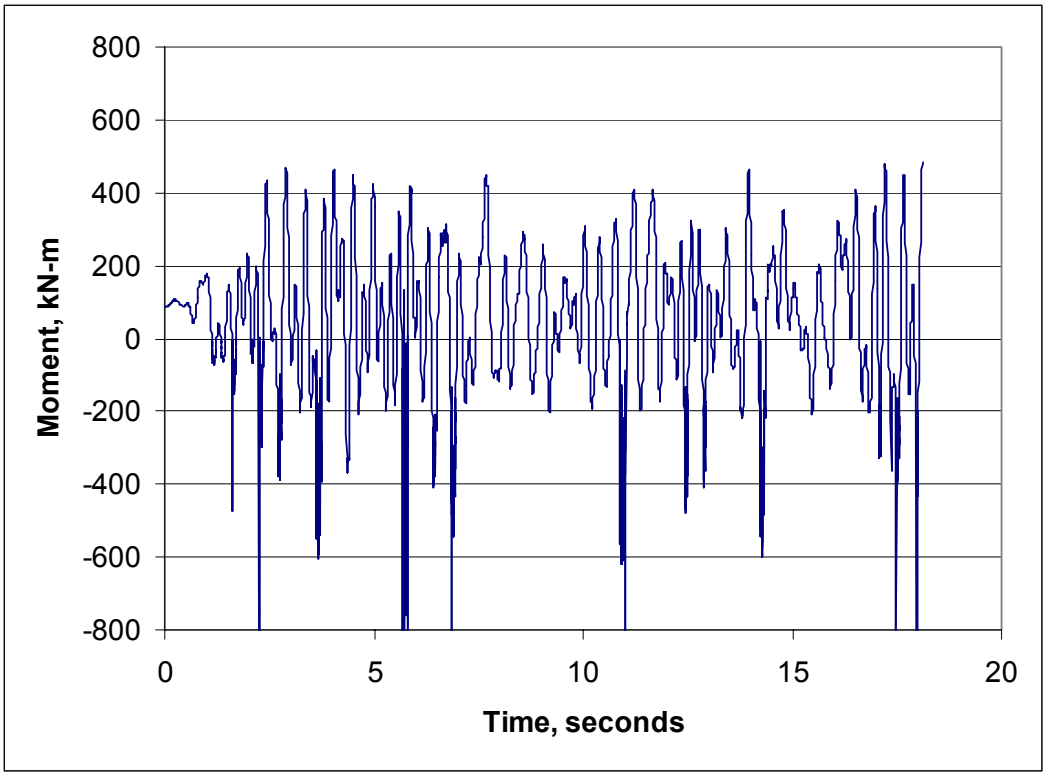

Figure C.16 Old (1993) IPIRG-2 Experiment 1-1 pretest design analysis moment-time results

worthwhile to document their use for the cracked pipe problem, because without them, generating solutions for arbitrarily oriented cracks may appear to be intractable.

C.3.3.1 Defining Crack Orientation

Figure C.17 shows a surge line running from the hot leg to the pressurizer of a Westinghouse 3-loop PWR plant in a perspective view. Also shown is the steam generator and the global reference coordinate system. Considering a case where a circumferential crack is to be analyzed at the hot leg to surge line intersection, looking at Figure C.17, it nominally appears as though the surge line is aligned with the global reference axes. However, looking at the system with orthogonal views aligned with the global axes, Figures C.18 to C.20, it is apparent that the surge line is definitely not aligned with the global axes: Moving away from the hot leg along the axis of the surge line, it drops down in Z, and it moves toward –X. Describing the directions associated with this geometry via Euler angles and coordinate rotations would be prone to mistakes, if not extremely difficult, whereas using the built-in local coordinate system capabilities of the finite element program is, comparatively, trivial.

ANSYS has a number of methods that can be used to define local coordinate systems, but the easiest one to use for illustration purposes is the node-based definition, i.e., CS command. Using this style of local coordinate definition, the local axes are completely defined by specifying the following:

1. The origin of the coordinate system is defined by selecting a node
2. The direction of the local X axis is defined by a second node
3. The direction of the Y axis is then defined by selecting a node in the X-Y plane.

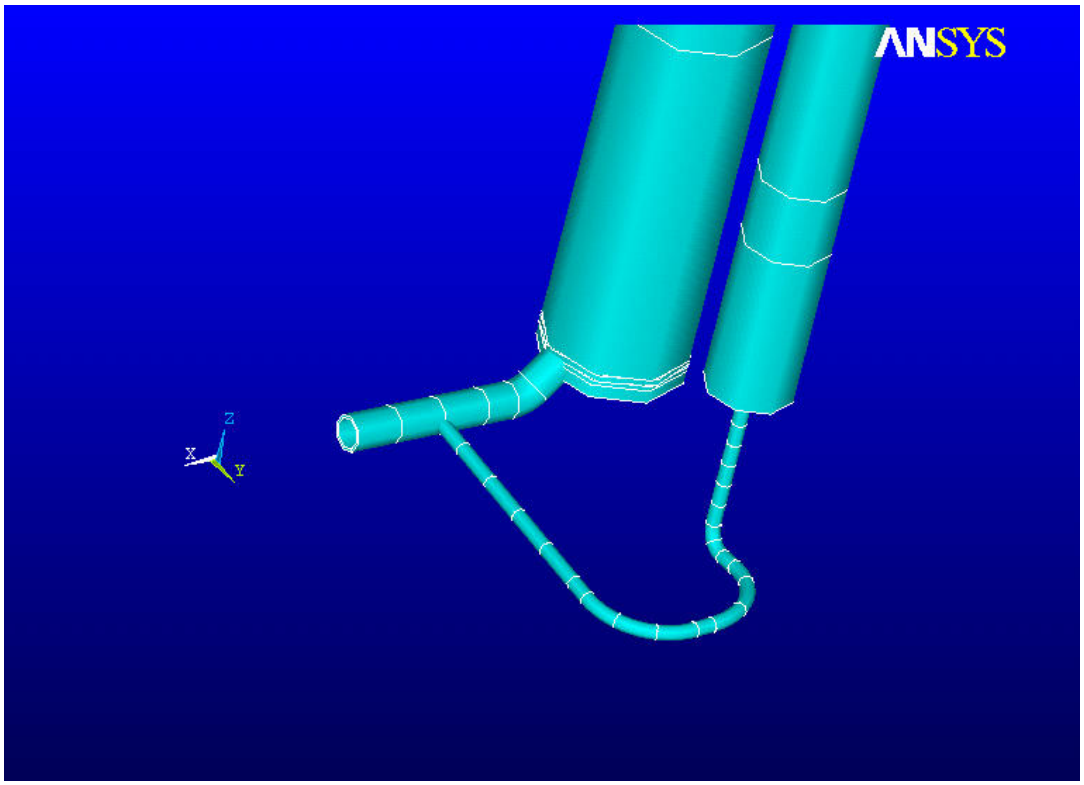

Figure C.17 PWR model surge line with global reference axes

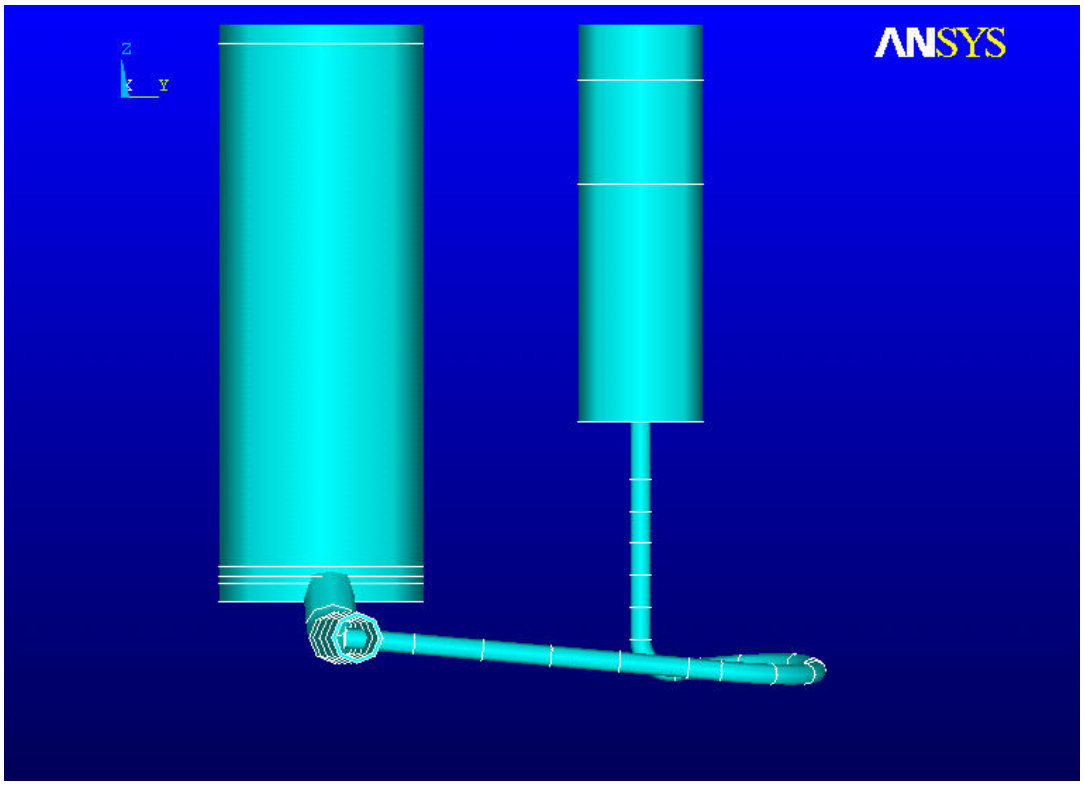

Figure C.18 Side view of the surge line

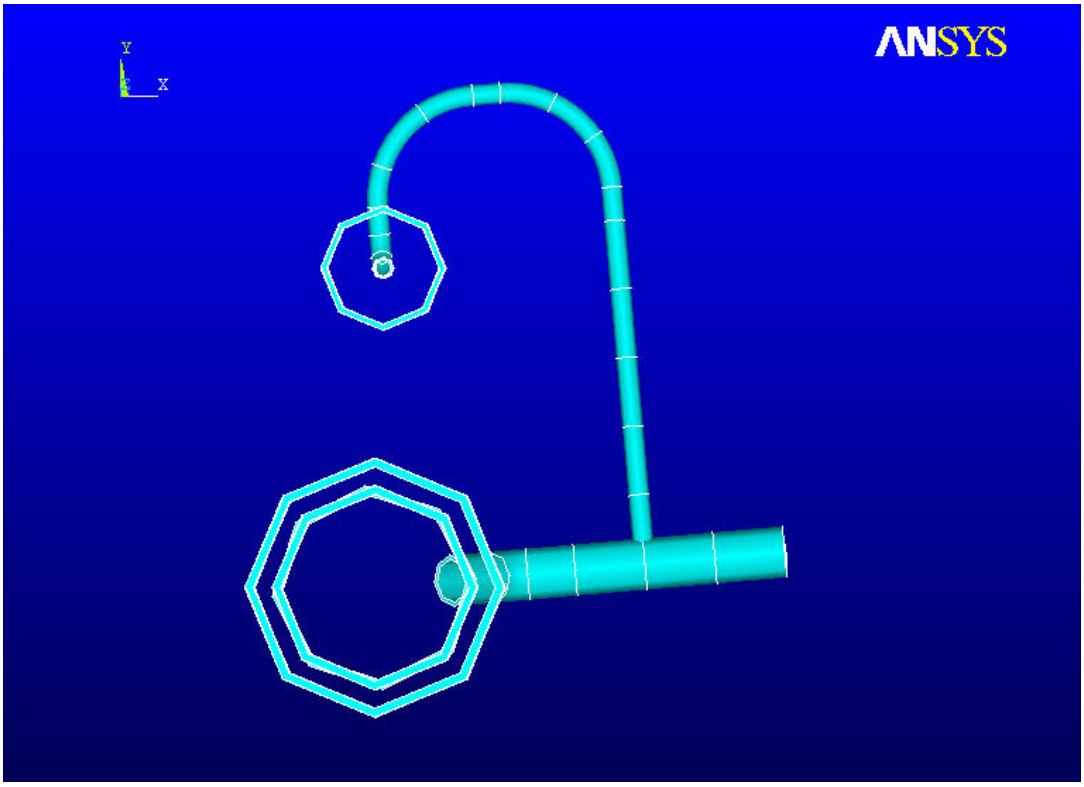

Figure C.19 Top view of the surge line

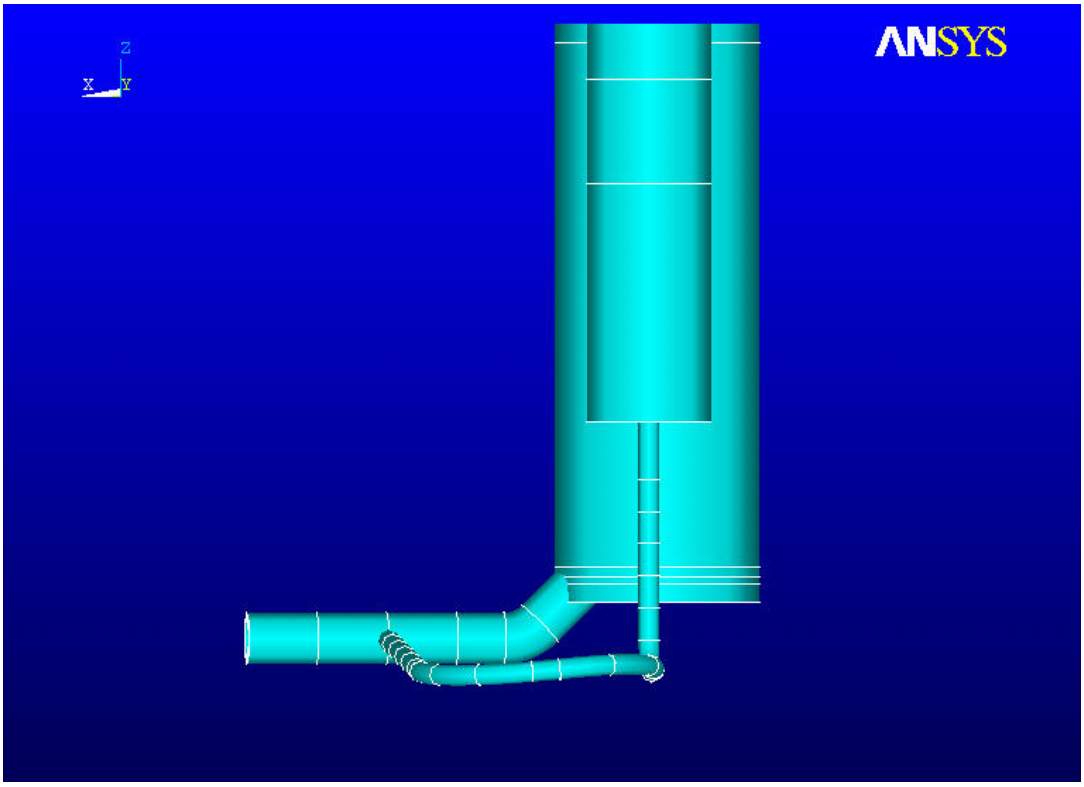

Figure C.20 Front view of the surge line

Given these three bits of information, a local coordinate system, with the X-axis directed along the axis of pipe can easily be defined, Figures C.21 and C.22. (Note: To define these axes, a dummy node was inserted at the X-Y coordinates of the end of the surge line but with a greater Z elevation.) To complete the local axis definition, the local coordinate system can be rotated about its own X axis with a CLOCAL command, compare Figures C.21 and C.23.

Given the local coordinate system, the coincident finite element nodes associated with the crack can be rotated into the local coordinate system (NROTAT command) and the crack springs and constraints defined in the local system just as though they were in the global reference system. Care must be taken when recovering crack rotations and moments to be sure which coordinate system they are in, but usually, these can be forced to be output in the local coordinate system.

C.3.3.2 Crack Orientation Summary

Being able to define the orientation of a crack oriented in any direction, relative to a global reference coordinate system, is essential to conducting nonlinear cracked pipe analyses. There are well-defined brute-force methods that can be applied, but the use of local coordinates greatly simplifies the work for the piping stress analyst.

Although the present discussion has focused on the local coordinate system facilities of ANSYS, any contemporary general purpose finite element program should have similar capabilities that a piping analyst needs to use to his/her advantage.

C.4 Analytical Study of Margins

There is a sense that nuclear power plant piping is far more tolerant of defects than the traditionally used linear analyses suggest. Heretofore, no systematic effort had been spent to determine just how much margin really exists in plant piping. The BINP Actual Margins task addressed this deficiency. By way of example, some idea of the margins that might be seen in plant piping was explored by looking at the margins that exist in two piping systems, namely the IPIRG pipe loop and the primary piping in a PWR plant. The conclusions from these examples can, by no means, be extrapolated to every plant piping situation, but they do provide a justification for continued consideration of the use of the nonlinear methods that are used to calculate these margins.

C.4.1 Analysis of IPIRG Pipe Loop Experiment Scenarios

As a preliminary to considering the margins in real plant piping, margins were calculated for the IPIRG pipe test system. The interest in the IPIRG pipe system was driven by a desire to know what might have been observed had the Actual Margins task had been conducted experimentally. To make the margins most apparent, the analyses were conducted assuming that the whole IPIRG pipe loop was made out of TP304 stainless steel and single frequency excitation loading was used.

C.4.1.1 IPIRG Analysis Model

Figure C.24 is an artist's rendition of the IPIRG pipe loop and Figure C.25 shows the physical dimensions of the pipe loop. Unlike the actual IPIRG pipe loop, all of the Actual Margins pipe, except for the cracked section, was assumed to be 406-mm (16-inch) nominal diameter Schedule 100 pipe. Also unlike the actual IPIRG pipe loop which had high-strength carbon steel elbows and straight pipe, the configuration analyzed assumed that all of the pipe was TP304 stainless steel.

Four different cracks were analyzed as shown in Table C.6. In every case, the cracks were assumed to be in base metal TP304 stainless steel pipe of the same size as tested in IPIRG-1 Experiment 1.3-3 (Refs. C.7 and C.8), i.e., 415.8-mm (16.37-inch) OD by 26.2-mm (1.031-inch) wall thickness. The cracks, as well as the rest of the pipe loop, were assumed to be at PWR conditions, i.e. 288°C (550°F) and 15.5 MPa (2250 psi). For the leak rate calculations, the through-wall cracks were assumed to be fatigue cracks, with an assumed nominal

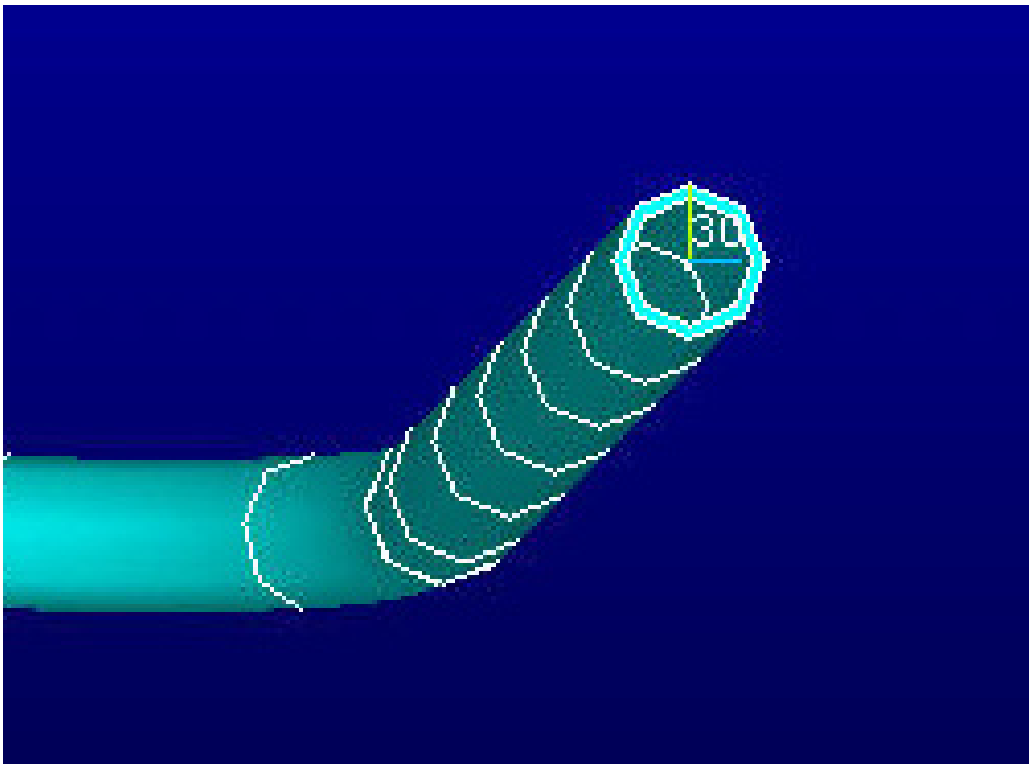

Figure C.21 View looking down the surge line, more or less along the #30 local coordinate system X axis

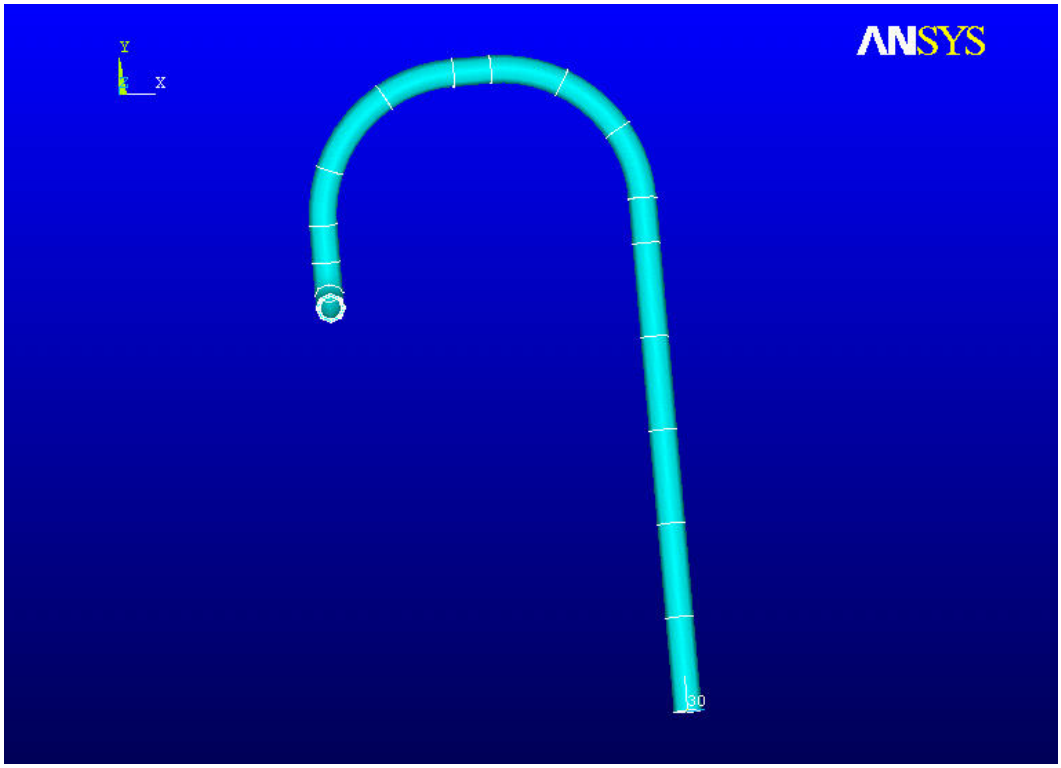

Figure C.22 Top view of the surge line showing local coordinate system #30

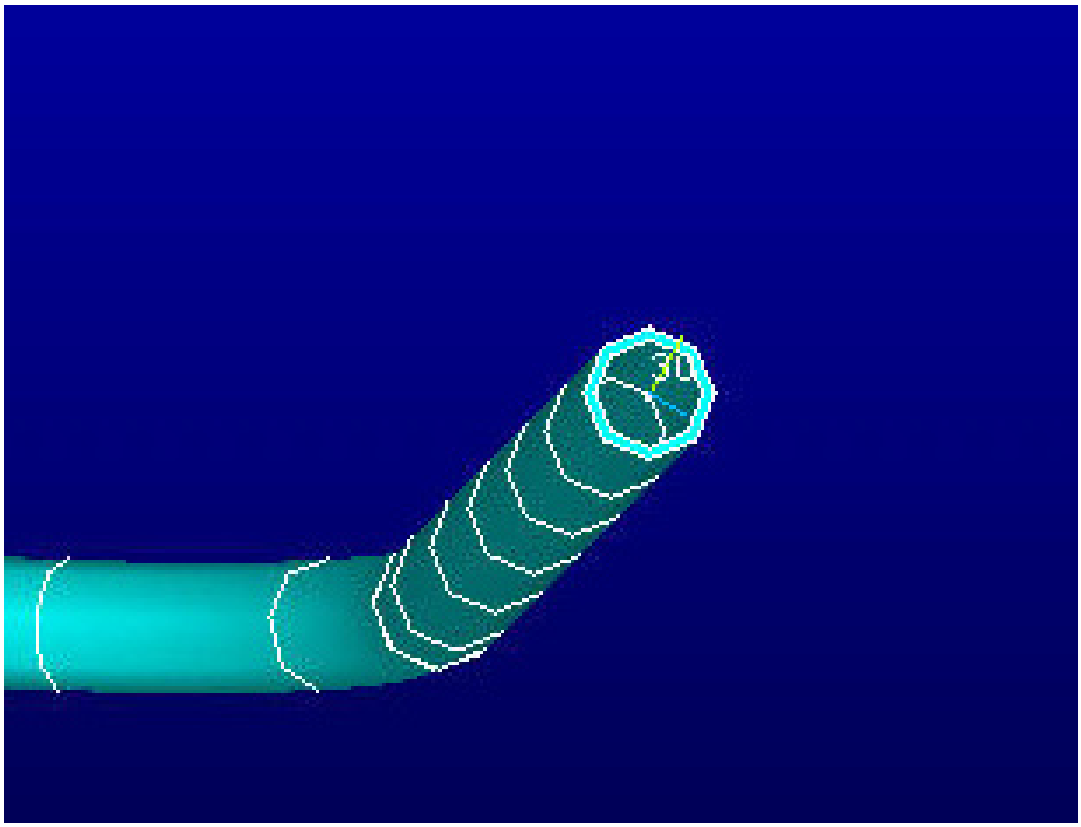

Figure C.23 View looking down the surge line, more or less along the rotated #30 local coordinate system X axis

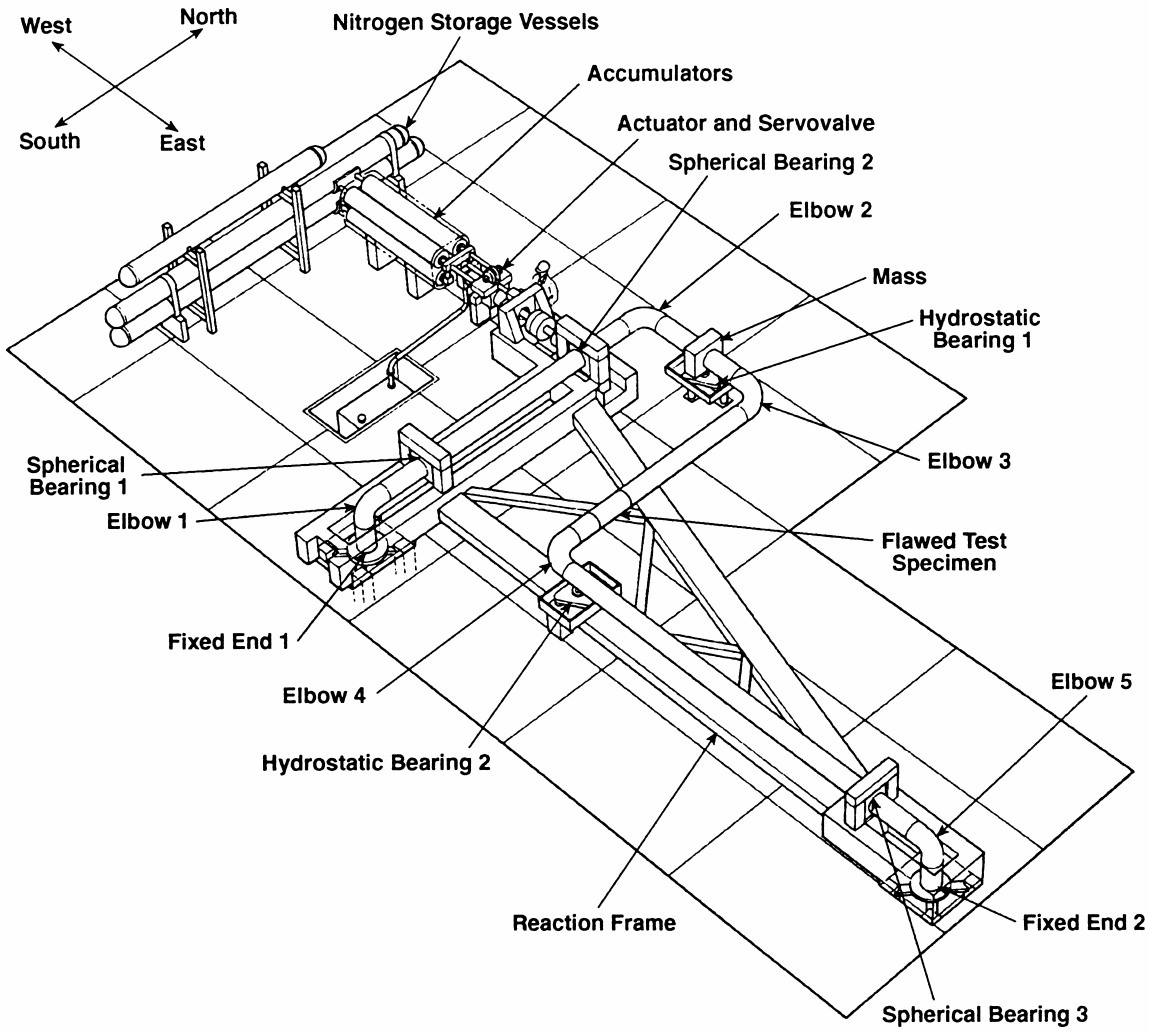

Figure C.24 Artist's rendition of the IPIRG pipe test facility

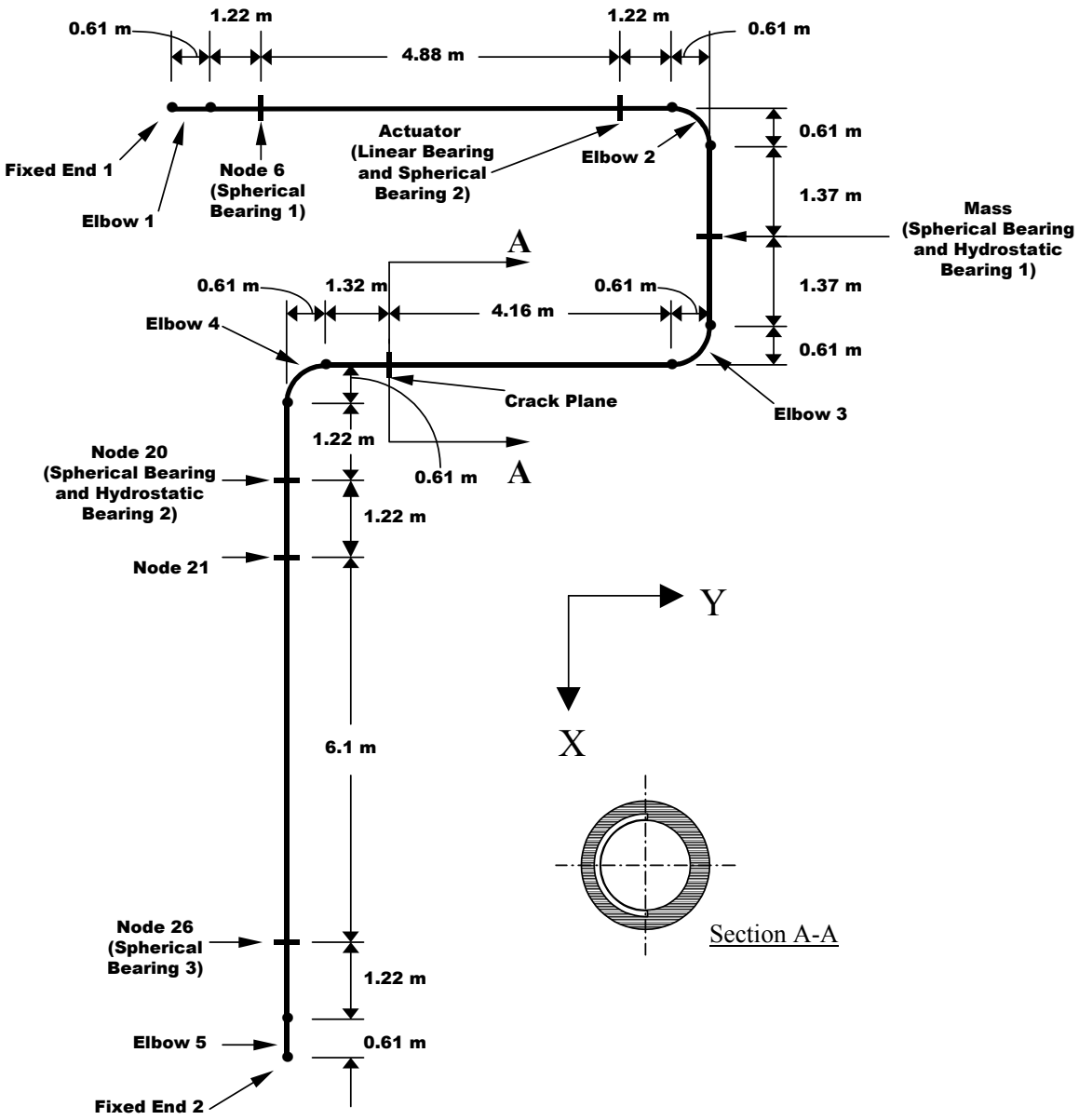

Figure C.25 Dimensions of the IPIRG pipe loop

Table C.6 IPIRG pipe loop system Actual Margins task cracks

Crack Description	Leak Rate liter/min (gpm)	Crack Size		Load Capacity kN-m (in-kip)
		Depth, d/t	Length, L/(πD)	
Large SC	-	0.66	0.50	459.2 (4064.4)
Small SC	-	0.48	0.50	651.5 (5766.1)
Large TWC	189.27 (50)	1.0	0.19	452.2 (4000.4)
Small TWC	18.9 (5)	1.0	0.09	679.6 (6015.5)

operating stress of S_m [116.9 MPa (16.95 ksi)]. Material properties for the cracks and the pipe remote from the crack were assumed to match A8ii-17 (Ref. C.9). NRCPIPE (Ref. C.10) was used to calculate the moment carrying capacity of the through-wall cracks and NRCPIPES (Ref. C.11) was used to calculate the moment carrying capacity for the surface cracks. SQUIRT (Ref. C.12) was used to do the though-wall crack leak rate calculations.

The applied load for these analyses were assumed to be the same single frequency, growing amplitude forcing function used in experiment IPIRG-1 1.3-3, see Figure C.26. In equation form, the applied displacement is:

$$\text{disp} = 0.375t + 9.5(1 - e^{-0.04042t})\sin 24.819t \quad \text{inches} \qquad \text{(C.13)}$$

This excitation is at about 90-percent of first resonance for the pipe loop, so it provides a great deal of dynamic amplification. Single frequency excitation was selected for the Actual Margins calculations so that attention could be focused solely on margin issues and not on crack closure behavior and ordering of load peaks in a seismic time history—the moment will be monotonically increasing, at least for a linear analysis.

A complete listing of the geometry for the model is given in section C.6.2.

C.4.1.2 IPIRG Cases

Four analyses were conducted for each of the four flaws as shown in Table C.7. These four cases consider all of the possible sources of margin from nonlinearities: plasticity due the crack, plasticity due to remote yielding, and the combined effect. Comparing each of the nonlinear cases with the linear case provides a sense of margin that each of the separate effects contributes to the total actual margin.

C.4.1.3 Calculation of Margins in the IPIRG Analyses

There are many ways to quantify margin in a piping stress analysis: Stresses can be compared, crack sizes that can sustain a certain applied moment, or a comparison of moments are a few that come to mind. In any event, the margin of interest comes from a comparison of what happens in a nonlinear analysis with what happens in a linear analysis. For the purposes of this discussion, comparison of moments seems appropriate. Furthermore, the comparison can be done several ways, but the simplest is to look at the ratio of the nonlinear moment to the linear moment, i.e.,

$$\text{margin} = \frac{M_{elast}}{M_{nl}} \qquad \text{(C.14)}$$

Margins greater than one imply that that the nonlinearity has mitigated the moment applied to the crack so that it is less likely to "fail."

Once a commitment has been made to discuss margin in terms of moment, the details of exactly how the margin is to be calculated have to be prescribed, because the margin is a continually evolving thing in time: For some portion of a time history of moment, a nonlinear and linear analysis will be identical so the margin will be 1.0, i.e., plasticity has not developed so there is no benefit from doing the nonlinear analysis. At some later point in time, however, if the excitation becomes large enough, there will be differences between the linear and nonlinear analyses that, presumably, should lead to margin. Issues such as time phasing of response will manifest themselves in the analysis results because nonlinearities look like damping to the rest of the pipe system. Because of the evolving nature of margin, one has to set "rules" for how the margin is to be calculated so that the comparisons are reasonable and fair.

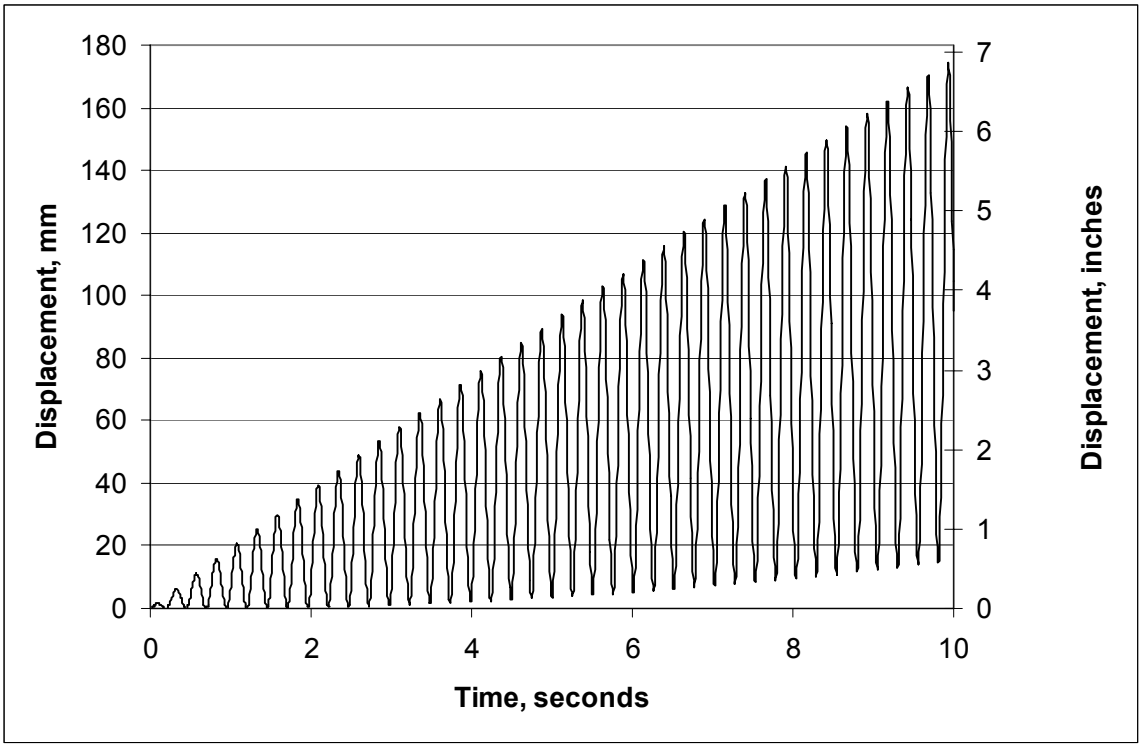

Figure C.26 Actual Margins forcing function used for IPIRG pipe loop analyses

Table C.7 IPIRG pipe loop system Actual Margins runs

Analysis	Crack	Remote Pipe Condition
1	No	Elastic
2	Yes	Elastic
3	No	Nonlinear
4	Yes	Nonlinear

For the purposes of this discussion the following rules were followed to calculate margins:

1. The maximum moment capacity for the crack, as calculated using the J–estimation schemes in NRCPIPE (Ref. C.10) or NRCPIPES (Ref. C.11), is the reference moment, M_{ref} .
2. A nonlinear analysis with a crack as the only nonlinearity is conducted to the time when the crack reaches its maximum moment carrying capacity.
3. The time at which maximum moment is attained is taken as reference time, $t1_{ref}$.
4. A nonlinear analysis with remote plasticity as the only nonlinearity is conducted to the time when the applied moment at the crack location reaches the reference moment defined in Step 1.
5. The time at which maximum moment is attained is taken as reference time, $t2_{ref}$.
6. A nonlinear analysis with a crack and remote plasticity is conducted to the time when the crack reaches its moment carrying capacity.
7. The time at which maximum moment is attained is taken as reference time, $t3_{ref}$.

8. A completely elastic analysis is conducted out to the maximum of $t1_{ref}$, $t2_{ref}$, or $t3_{ref}$ times.
9. Margins are calculated as follows:

$$\text{margin}_{\text{Crack}} = \frac{M_{elast}(\max \text{ from } t = 0 \text{ to } t1_{ref})}{M_{nl}(t1_{ref})} \quad \text{(C.15a)}$$

$$\text{margin}_{\text{Remote Plasticity}} = \frac{M_{elast}(\max \text{ from } t = 0 \text{ to } t2_{ref})}{M_{nl}(t2_{ref})} \quad \text{(C.15b)}$$

$$\text{margin}_{\text{Plasticity+Crack}} = \frac{M_{elast}(\max \text{ from } t = 0 \text{ to } t3_{ref})}{M_{nl}(t3_{ref})} \quad \text{(C.15c)}$$

C.4.1.4 IPIRG Analysis Results

Analyses were conducted for the four flaws described in C.4.1.1 in accordance with the "rules" defined in C.4.1.3 for an all stainless steel IPIRG pipe system geometry with a single frequency, increasing amplitude forcing function. Figures C.27 through C.31 show the moment-time plots for all of the runs. As expected, the moment grows monotonically with time for the linear analysis. For the plasticity only case, the moment reaches a plateau in approximately two seconds that is almost never exceeded. In this case, plasticity initiates in elbow 2 and subsequently appears in elbow 3 and at the actuator location, as well as a slight amount at the hanger near fixed end 2 (see Figures C.24 and C.25). For several of the cases with remote plasticity, the crack location never reaches the "failure" moment.

Table C.8 summarizes the margins that are implied by Figures C.27 though C.31.

C.4.1.5 Conclusions From the IPIRG Pipe System Margin Analyses

Inspection of the margins listed in Table C.8 shows that virtually all of the margin from these analyses comes from plasticity remote from the crack and that the margin effects of the crack nonlinearity and remote plasticity are not additive. Furthermore, it is apparent that these conclusions are true, independent of the whether the crack is a through-wall crack or a surface crack. Some of the crack-only cases yielded margins less than one, but these cases have "failure times" very early on, when transient behavior is dominating the pipe response. For several cases, the reference moment was never attained within the time frame of the analysis. Remote plasticity was taking so much energy away from driving the crack that the crack was never loaded to failure in a ductile tearing episode. Low cycle fatigue would need to be considered in these cases.

The results of these calculations suggest that it is not terribly important to have a crack in the piping model, because the vast majority of the margin comes from remote plasticity. Indeed, this is an unexpected, but positive result, because it makes a nonlinear analysis much simpler to conduct: The issues related to defining crack springs, crack unloading, and crack orientation become moot—there is no need to put a crack in the model.

C.4.2 Analysis of PWR Plant Piping

The results presented in C.4.1 provide a tantalizing view of the margins that may be available in flawed plant piping. Clearly, in a situation where linear analysis shows that a flaw evaluation or LBB assessment has inadequate margin, adequate margin may in fact actually exist if the effort is made to do a nonlinear analysis. The results from the previous section seem to indicate that a cost-benefit may be there, if there is a compelling need to find additional margin.

The analyses presented in C.4.1 are rather idealized: The IPIRG pipe system has unrealistic boundary conditions and the loading was monotonically increasing. To see if the margins observed in C.4.1 can be realized in real plant piping, analyses consistent with what was done in C.4.1 but using real geometry, boundary conditions, and real seismic loading were performed.

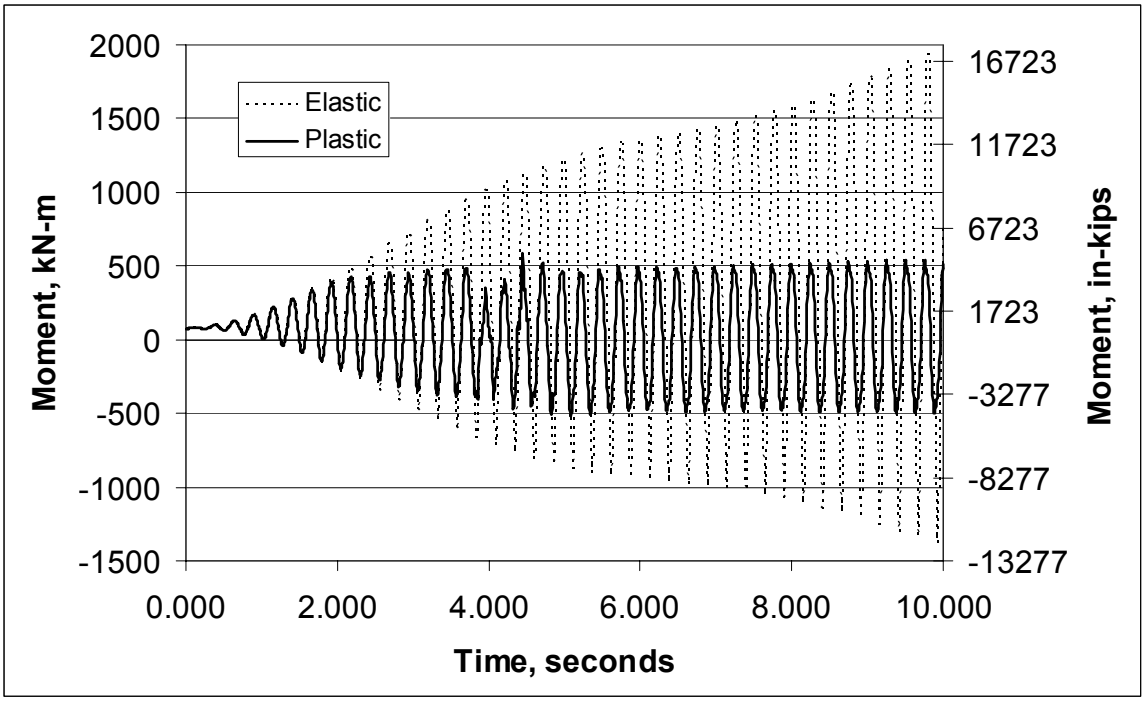

Figure C.27 IPIRG pipe system reference moments

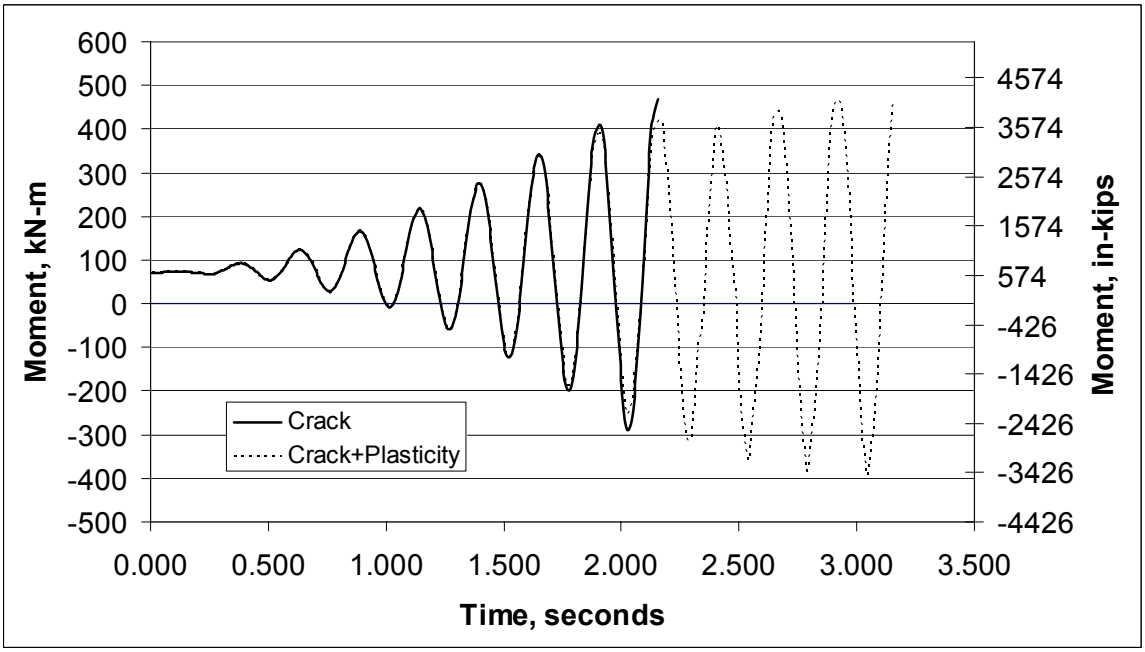

Figure C.28 IPIRG pipe system large surface crack results

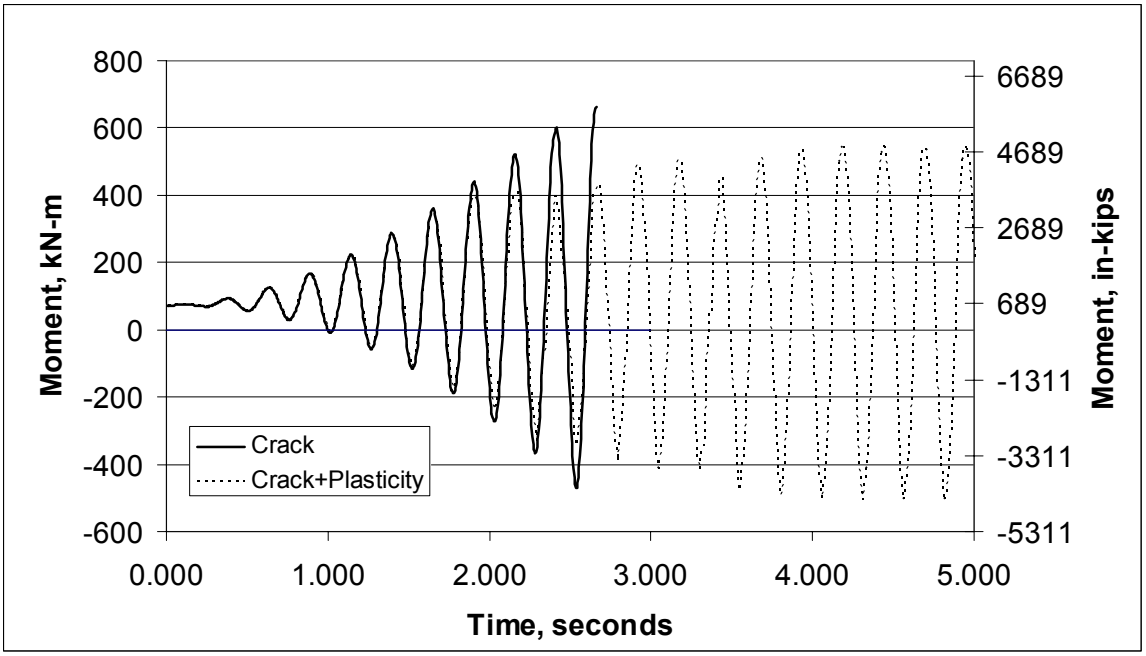

Figure C.29 IPIRG pipe system small surface crack results

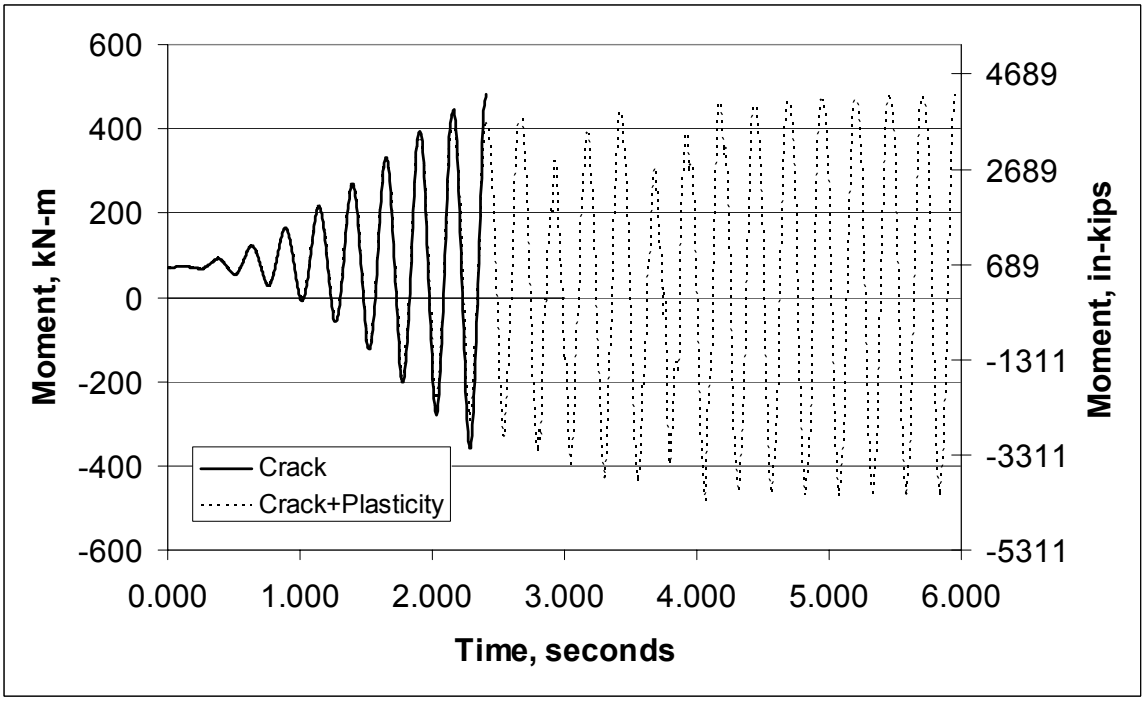

Figure C.30 IPIRG pipe system large through-wall crack results

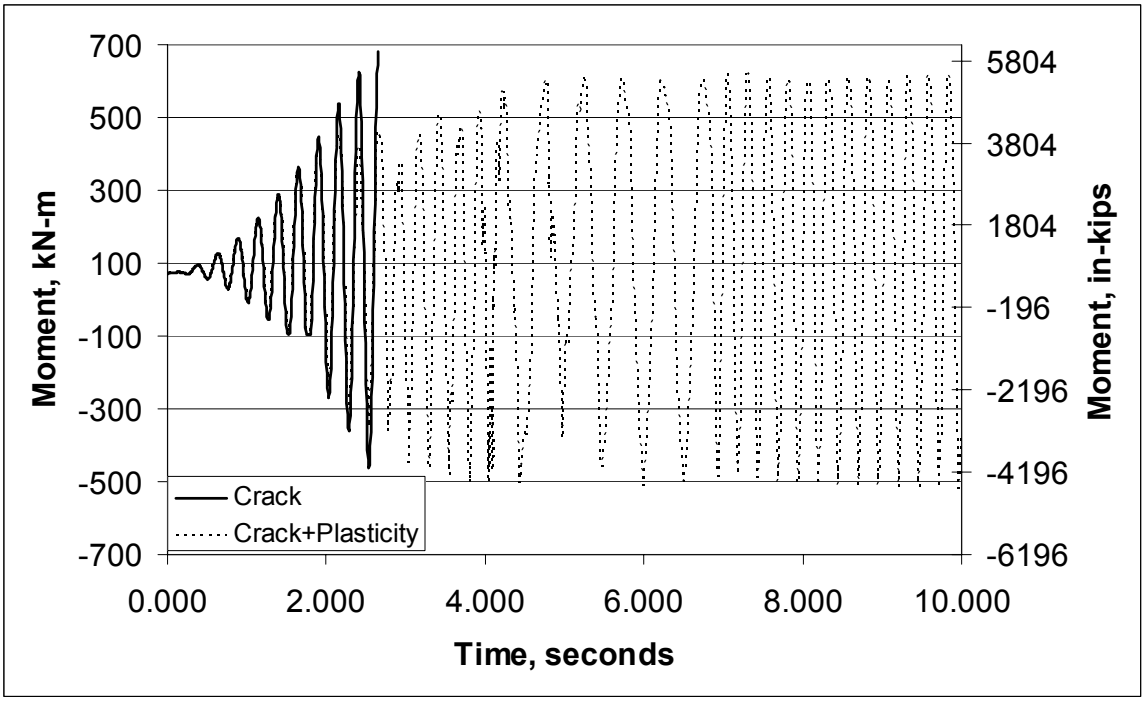

Figure C.31 IPIRG pipe system small through-wall crack results

Table C.8 IPIRG pipe system analysis margins

Condition	Crack		Large SC	Small SC	Large TWC	Small TWC
	M_{ref}	kN-m	459.2	651.5	452.2	679.6
		(in-kips)	(4064.4)	(5766.1)	(4002.4)	(6015.5)
Crack Only	$t1_{ref}$,sec		2.155	2.660	2.410	2.655
	M_{elast}	kN-m	438.0	572.1	500.5	571.7
		(in-kips)	(3876.5)	(5064.0)	(4430.0)	(5060.0)
	margin1		0.95	0.88	1.11	0.84
Remote Plasticity Only	$t2_{ref}$, sec		3.185	DNF*@5	2.685	DNF*@10
	M_{elast}	kN-m	759.3	1218.3	648.5	1943.3
		(in-kips)	(6720.4)	(10782.9)	(5740.0)	(17200.0)
	margin2		1.65	2.08	1.43	3.31
Crack+Plasticity	$t3_{ref}$, sec		2.920	DNF*@5	5.955	DNF*@10
	M_{elast}	kN-m	651.5	1218.3	1333.2	1943.3
		(in-kips)	(5766.6)	(10782.9)	(11800.0)	(17200.0)
	margin3		1.42	1.75	2.95	2.71

DNF = did not "fail"

C.4.2.1 Development of a Plant Piping Model

In order to perform margin calculations for plant piping, a plant piping model that includes all of the features relevant to loading of the pipe must be available or developed. Features that were judged to be of first order significance in the dynamic behavior of PWR plant piping are:

- All primary loops:
  - The piping
  - Coolant pumps and support
  - Steam generator and support
- The reactor
- The surge line with hangers
- The pressurizer and its support
- Concrete inside containment
- The containment
- The plant base mat
- The soil

For each of these features, detailed geometry, properties including mass, section properties, and material properties, as well as boundary conditions (supports and applied SSE loading) must be known.

When the Actual Margins task was originally proposed, the hope was that one of the participants would be able to supply some or all of the plant data listed above. The reality was that the model had to be developed from scratch from publically available documents and some reasonable engineering guesses. Specifically, the data sources available for building the model were limited to US NRC Final Safety Analysis Reports (FSAR's), several internet web sites, NUREG reports, some soil-structure interaction software user's manuals, and conversations with NRC staff (Refs. C.13 through C.17). After some preliminary investigations, a three-loop Westinghouse PWR was selected for analysis because there appeared to be a wealth of the required information contained in some of the FSAR's. In addition, internet searches for information on nuclear plant construction details turned up a great deal of useful information for Westinghouse 3-loop plants.

The basic premise for developing the model was as follows:

1. The model was to be built from simple beam-type elements and springs/dampers
2. Consideration would only be given to analyzing the 3 primary loops, the surge line, and one safety injection system (SIS) line
3. The structural detail of the piping would be as precise as the available data would permit
4. The structural detail of the reactor foundation, containment, and internal concrete supports would only need to be good enough to adequately represent the mass and gross stiffness
5. In most cases, details of the piping hanger and other piping attachments to the building would be unknown and would have to be modeled as rigid connections
6. A simple linear spring and damper soil model would be used
7. If precise data for mass and stiffness of certain features was not available, informed engineering guesses would be made based on the best available information and/or scaled from pictures and artist's renditions.

The overriding consideration in developing the model was to do a very good job modeling the piping of interest and to make the rest of the model representative enough that it could be judged to have provided reasonable boundary conditions for the piping. Every attempt was made to rationalize mass and stiffness properties with other publically available data.

C.4.2.2 Plant Model and Loading Details

Figures C.32 to C.40 show various features in the plant and how they were modeled in the finite element model. In most cases, features were modeled with circular cross-section beams. Mass properties of the beams were adjusted to give the correct total mass and mass distribution.

Linear soil springs and dampers (Ref. C.18 and C.19) were selected to model a rock foundation. Consistent with the stiff, rock foundation assumption, the natural frequencies for the

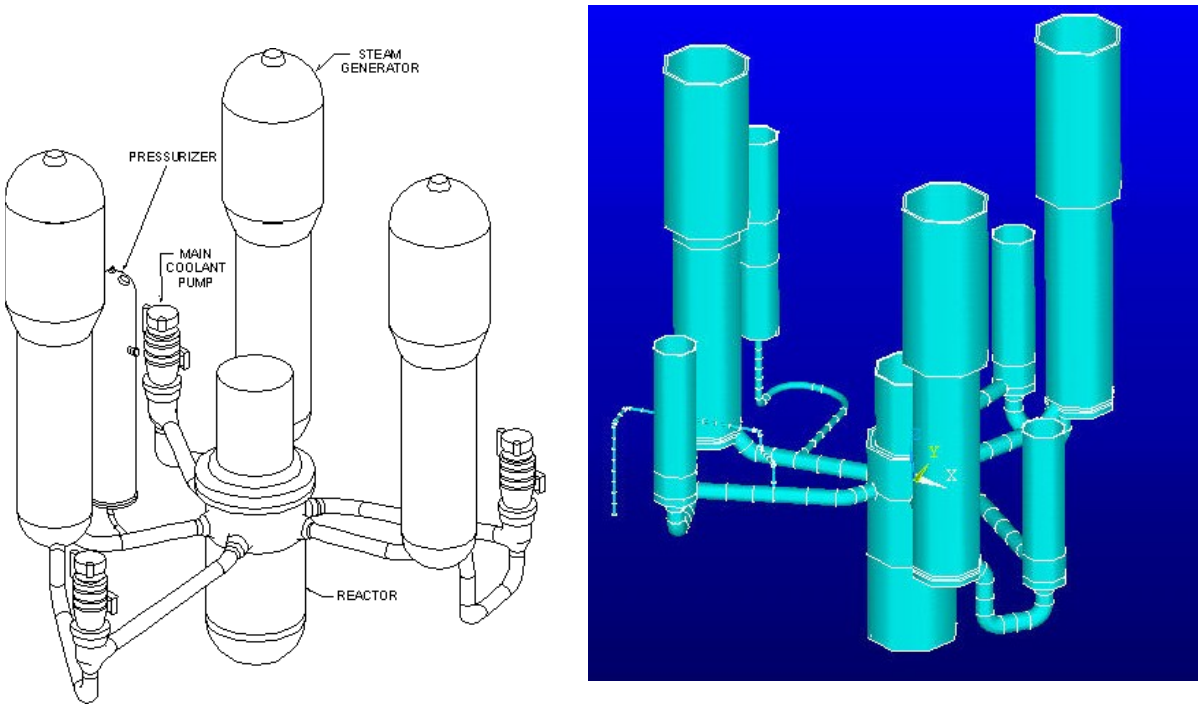

Figure C.32 PWR system model piping

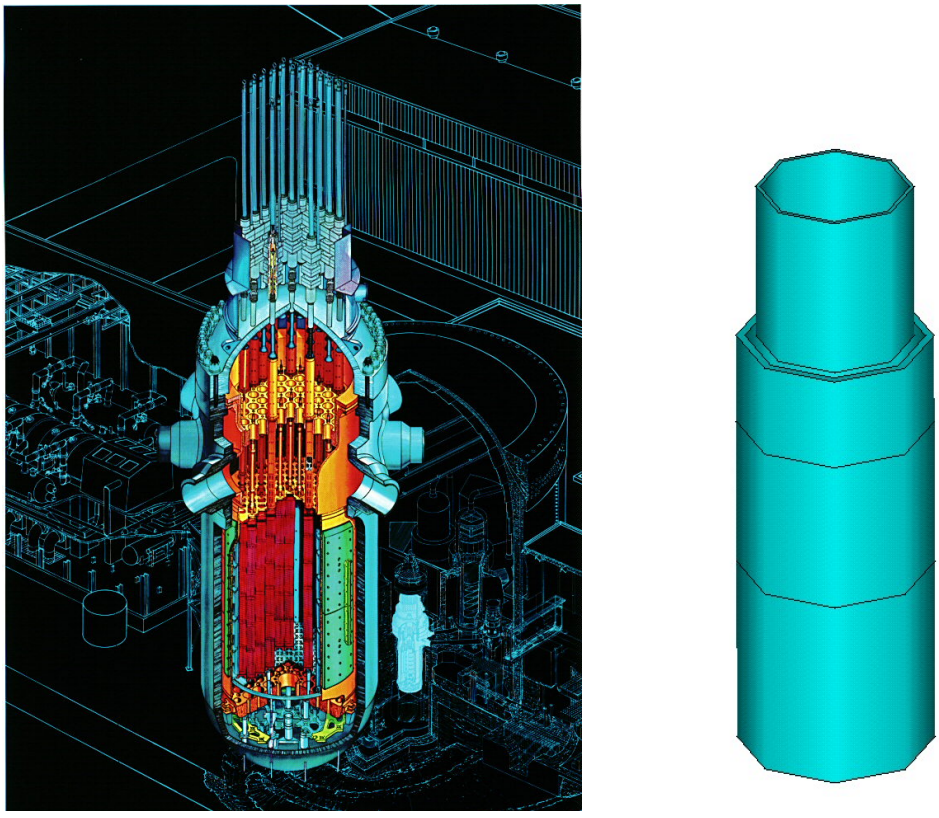

Figure C.33 PWR System Model Reactor

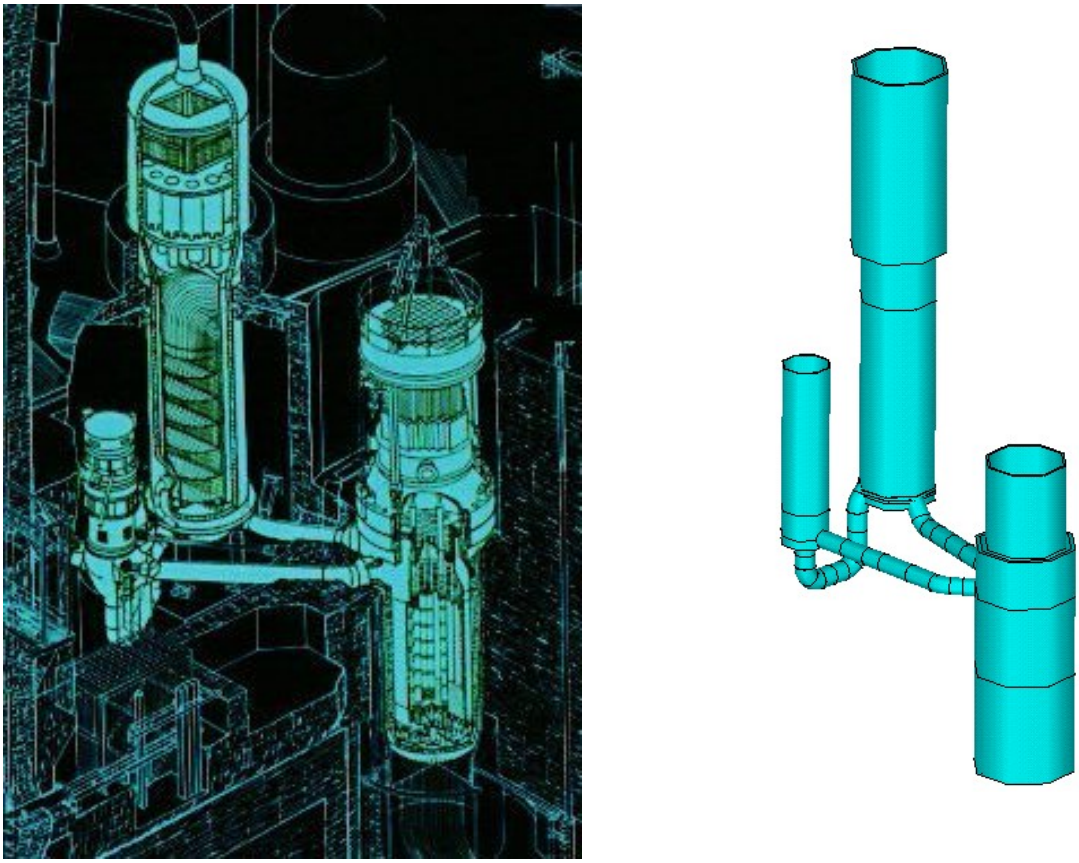

Figure C.34 PWR system model primary loop (one of three)

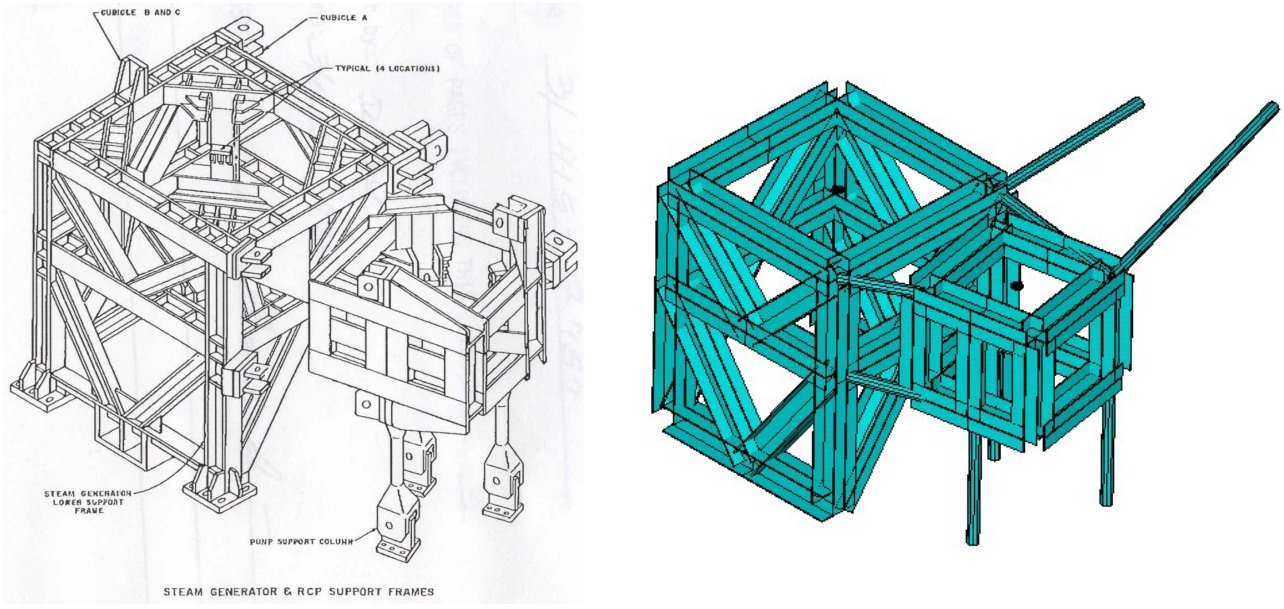

Figure C.35 PWR plant model stream generator and coolant pump support

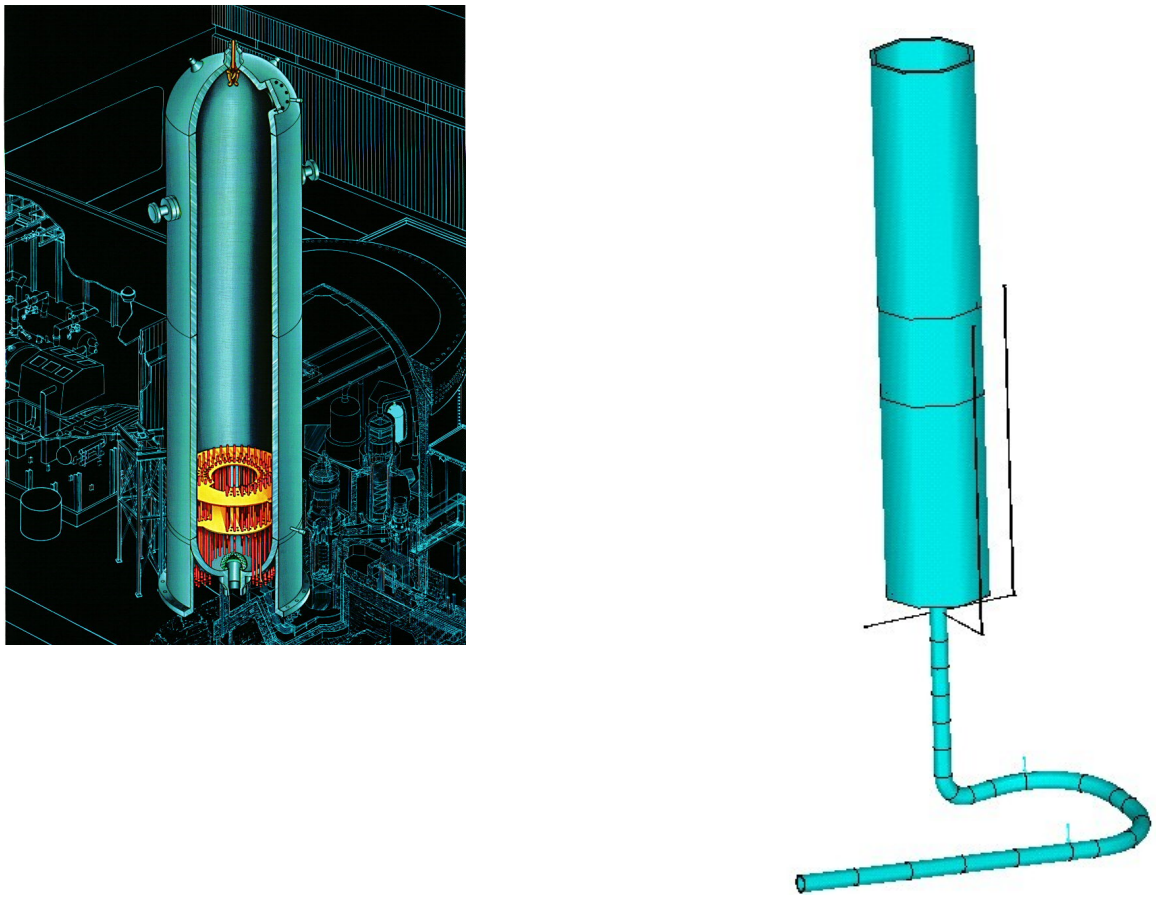

Figure C.36 PWR plant model surge line and pressurizer

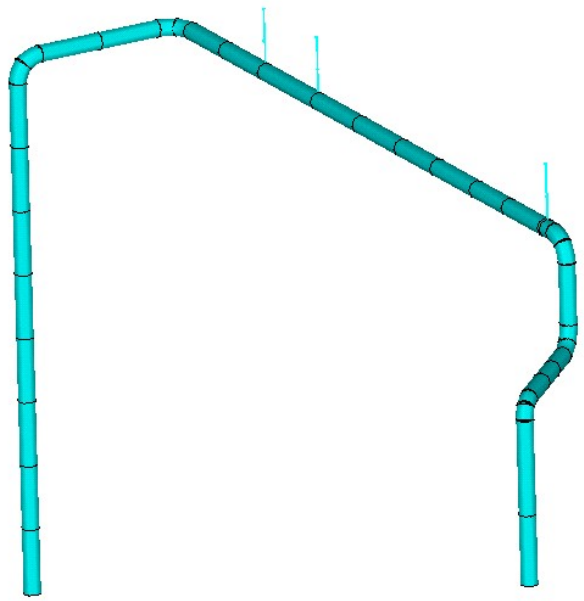

Figure C.37 PWR system model safety injection system (SIS) line

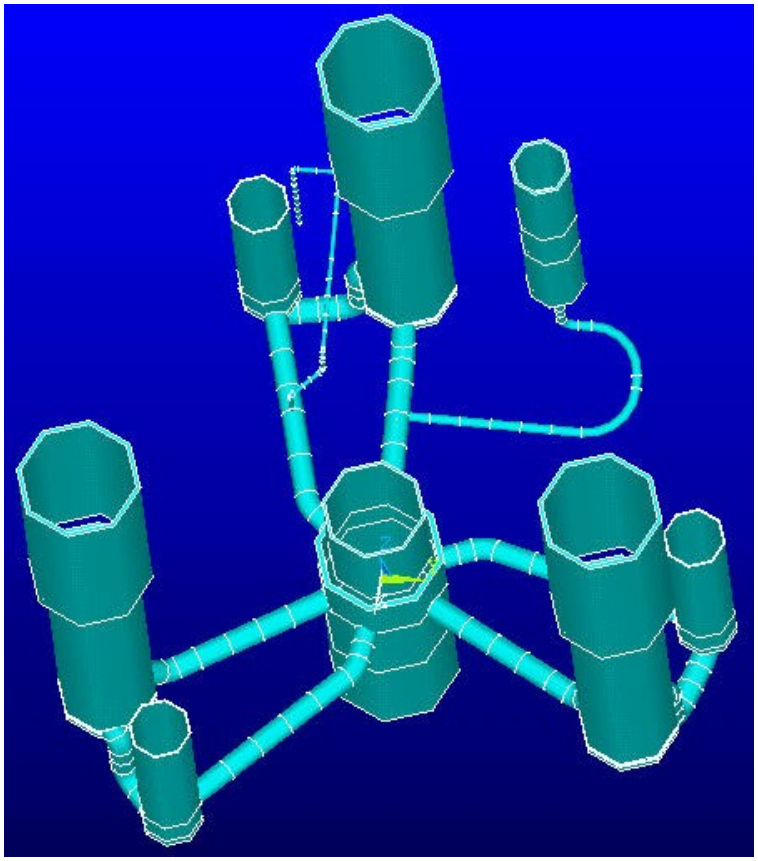

Figure C.38 PWR system model piping

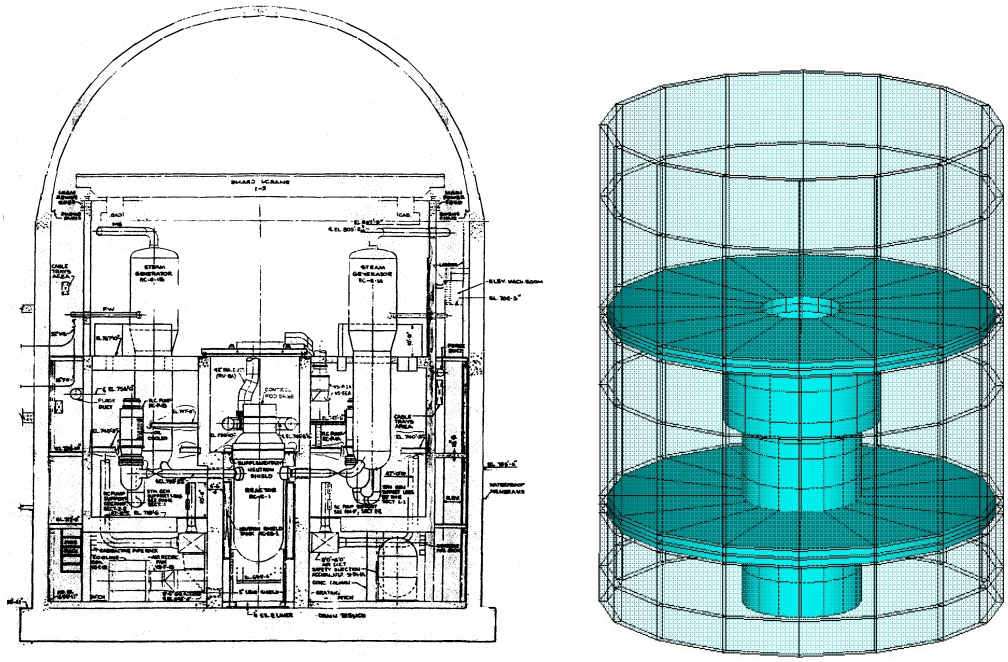

Figure C.39 PWR system model containment building internal concrete

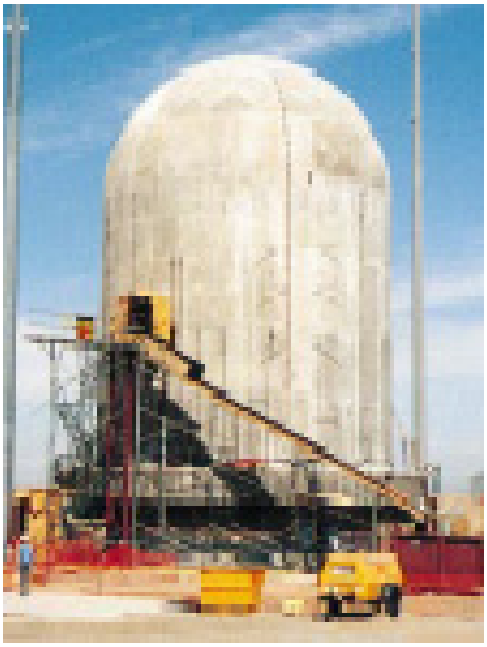

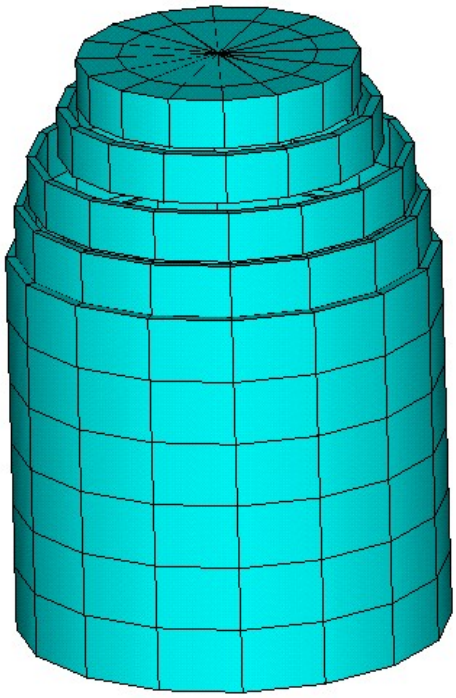

Figure C.40 PWR system model containment

reactor base mat, containment, and internal concrete, reactor core and piping are as follows:

- F_1=3.096 Hz, synchronized rocking of the containment and internals about the base mat
- F_2=3.980 Hz, rocking of the containment about the base mat with the internals relatively stationary
- F_3=5.151 Hz, a mode very similar to mode 2
- F_4=5.206 Hz, out of phase rocking of the containment and the internals about the base mat
- F_5=8.654 Hz, rocking of the internals about the base mat with the containment relatively stationary
- F_5=9.681 Hz, vertical in-phase motion of the containment and internals.

These frequencies are consistent with other published data for nuclear plant building natural frequencies (Refs. C.20 through C.22).

The input loading to the plant model was a scaled earthquake applied as acceleration loading in the global X and Y direction. The basic ground motion records, obtained from References C.23 and C.24, are derived from the 1988 Saguenay earthquake and represent a 5.9 magnitude earthquake at a distance of 96 km (60 miles) from the epicenter. This earthquake is characterized as having a 2-percent chance of exceedance in 50 years for the Boston, USA area, and has a peak acceleration of 0.57 g in the X direction and 0.78 g in the Y direction, see Figures C.41 and C.42. To put this excitation in perspective, Figure C.43 shows the SSE earthquake for the Beaver Valley PWR (a 3-loop Westinghouse design), taken from the Beaver Valley FSAR (0.13 g peak acceleration). The 2-percent in 50 years in Boston excitation is similar in duration and basic character, but is substantially more severe in magnitude. The two orthogonal components of the earthquake excitation were applied aligned with the global model reference axes. The decision to orient the earthquake in this direction is completely arbitrary and may have had some impact on the stresses generated in the piping.

The model has 1446 degrees-of-freedom and the seismic loading was applied at time steps of 0.005 second.

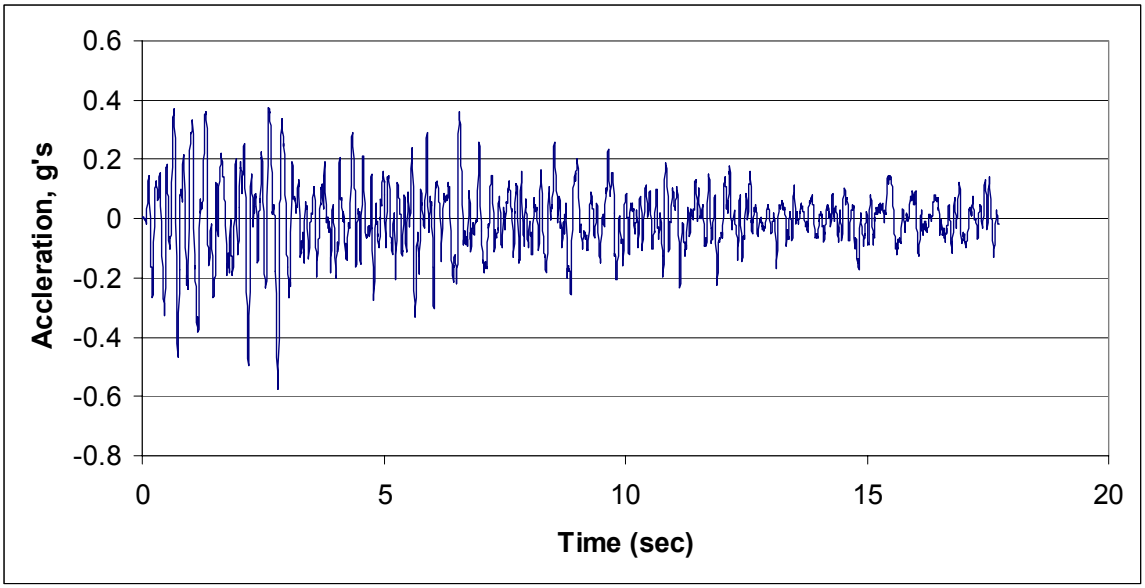

Figure C.41 PWR model X-axis loading

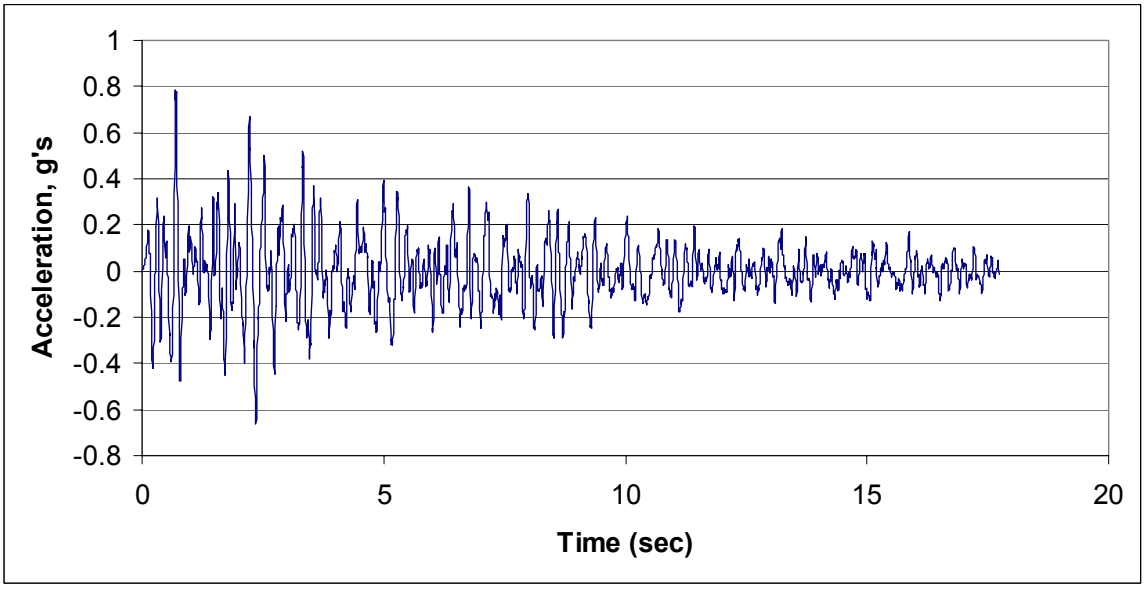

Figure C.42 PWR model Y-axis loading

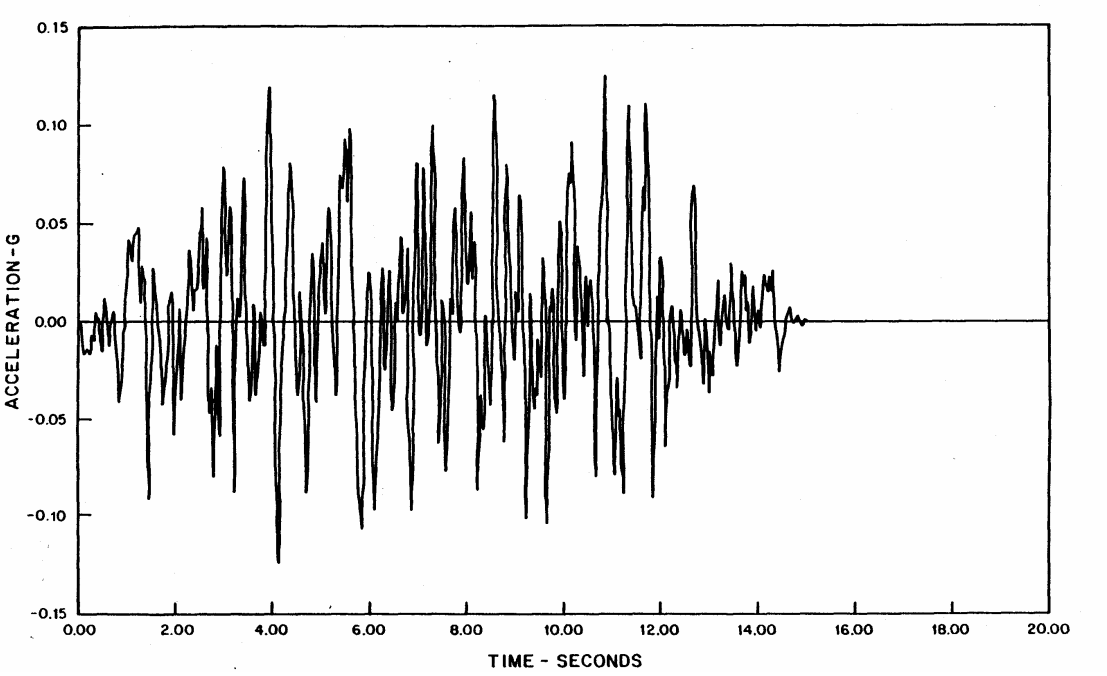

Figure C.43 Beaver Valley PWR artificial time history horizontal SSE (Ref. C.16)

C.4.2.3 Calculation of Margin for the PWR Piping System

The IPIRG pipe system margin calculations compared nonlinear moments with elastic moments over a window of time from t= 0 to the time when the hypothesized cracks reached maximum moment carrying capacity. Based on the conclusions of these analyses, it was determined that the crack does not contribute significantly to the margin, so one can merely compare linear solutions and solutions with remote plasticity to learn something about margins in real plant piping. Additionally, further simplification can be introduced by ignoring time-phasing of moment response, crack orientation and crack location issues by comparing the maximum magnitudes of bending moments (square root of the sum of the squares) for the full duration of the seismic event at many possible critical locations. In a real margin analysis it would be necessary to consider the real crack orientation at a specific location, but for the purposes of this study, these issues can be ignored.

Margin is a function of the level of applied loading. The general sense is that margin should be 1.0 at very low levels of excitation and grow as the excitation gets larger. It is conceivable that margin may not increase monotonically at all locations due to the interaction among various pieces of the piping. In order to explore the evolution of margin with changing seismic excitation, the basic seismic load can be linearly scaled. At a scale factor of 0.25, the 2-percent in 50-year Boston excitation is still 50-percent larger than the Beaver Valley SSE in terms of peak g's. Furthermore, it is clear that the margin will also be a function of the phasing of the peaks of the seismic excitation and the direction of the excitation. In the present case, the phasing and direction have been arbitrarily fixed by choice of the specific seismic signature.

In summary, the demonstration margins for the PWR plant analyses were calculated on the following basis:

- $\text{Margin} = \dfrac{M_{elastic}}{M_{nonlinear}}$
- $M = Max\left(\sqrt{M_y^2 + M_z^2}\right)_{t=0}^{t=18}$, i.e. maximum of the square root of the sum of the squares of the bending moments for the full duration of the seismic loading.

- The margin calculation is performed at every piping run end and every straight pipe to elbow junction.
- Margin is calculated as a function of increasing, scaled amplitude seismic excitation.

C.4.2.4 PWR Model Analysis Results

Figures C.44 to C.47 show the locations where margins were calculated according to the procedures defined in Section C.4.2.3. Figures C.48 to C.52 show calculated margins as a function of load. The figures show the results for all of the locations in each line, with the mean value shown as a block and the length of the line going from the highest to lowest margin at a particular excitation level. The calculated margins are a function of the specific location in a line, the direction of the applied excitation, and the exact character of the forcing function itself. Because only one excitation direction with one forcing function was actually analyzed, the data have been presented as bar charts to illustrate the potential margins that might be achieved: Different directions of excitation and/or different forcing functions may yield different results. For the hot leg, cross-over leg, and cold leg, results for all three loops are included in the respective figures.

Looking at the hot leg margins, Figure C.48, it is clear that: a) For the vast majority of locations, the average margin is at or near 1.0, b) Margin does not necessarily grow monotonically with increasing forcing function amplitude, and c) At excitation levels around typical SSE levels (0.1 < scale factor < 0.5), some locations can have high margins.

The comments regarding the cross-over legs (Figure C.49) are consistent with the preceding hot leg comments with the exception that there is a more pronounced increase of margin with increasing amplitude excitation. Observations about the margins for the cold leg (Figure C.50) are identical to the hot leg.

The margins for the surge line (Figure C.51) are unique among all of the margins in that they are all generally much higher than the others and, in the range of typical SSE peak g accelerations (0.1 < scale factor < 0.5), the margins can be very high. The extreme margin for the surge line occurs at the beginning of the last elbow leading to the pressurizer.

For the one safety injection system line (Figure C.52) analyzed (there are many more in the plant), the location at the hot leg exhibits the largest margins. For the vast majority of the other locations in the SIS line, the margin hovers in the range of 1.1 to 1.5.

As indicated at the beginning of this section, the results presented here are only a demonstration of potential margins that might exist: A different seismic loading from a different direction may show more or less margin.

C.4.2.5 Conclusions From the PWR Plant Piping Analyses

The PWR plant analyses demonstrated that margin can exist in actual plant piping. Within the limitations of the finite element model, assumed loading, and necessary simplifying assumptions, the vast majority of locations exhibited margins around 1.1. Some locations, however, exhibited margins greater than 10. The results shown here are indeed consistent with the results from the IPIRG pipe system analyses, but are, perhaps, not quite as dramatic. The results do, however, reinforce the notion that if there is a location in plant piping where a flaw evaluation or LBB assessment shows inadequate margin, one can have some reasonable assurance that if a nonlinear analysis is conducted, some increased margin will be found.

C.4.3 Task Summary

The Actual Margins task has demonstrated, at least on a limited scale, that conducting nonlinear dynamic finite element analyses can, in all likelihood, lead to enhanced margins. Using the latest techniques for nonlinear analysis, such as a good model for crack unloading and taking advantage of tools within finite element programs to help define crack orientation, as long as the basic program's plasticity calculations are sound, margin can be found, if it exists. Admittedly, the analyses are far more difficult than linear analyses: The analyst needs stress-strain data at temperature for the remote plasticity calculations and a J-R curve plus stress-strain data in order to consider the effect of cracks. Furthermore, the analyses, since they are

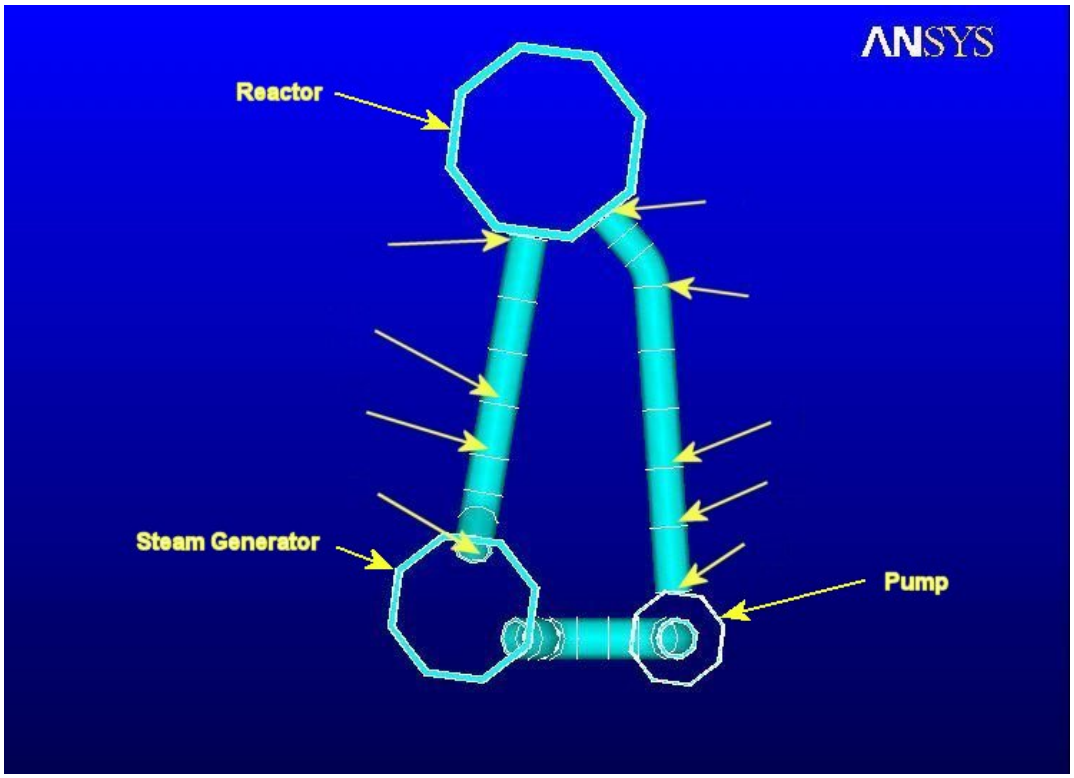

Figure C.44 PWR primary piping margin evaluation locations, 1 of 2

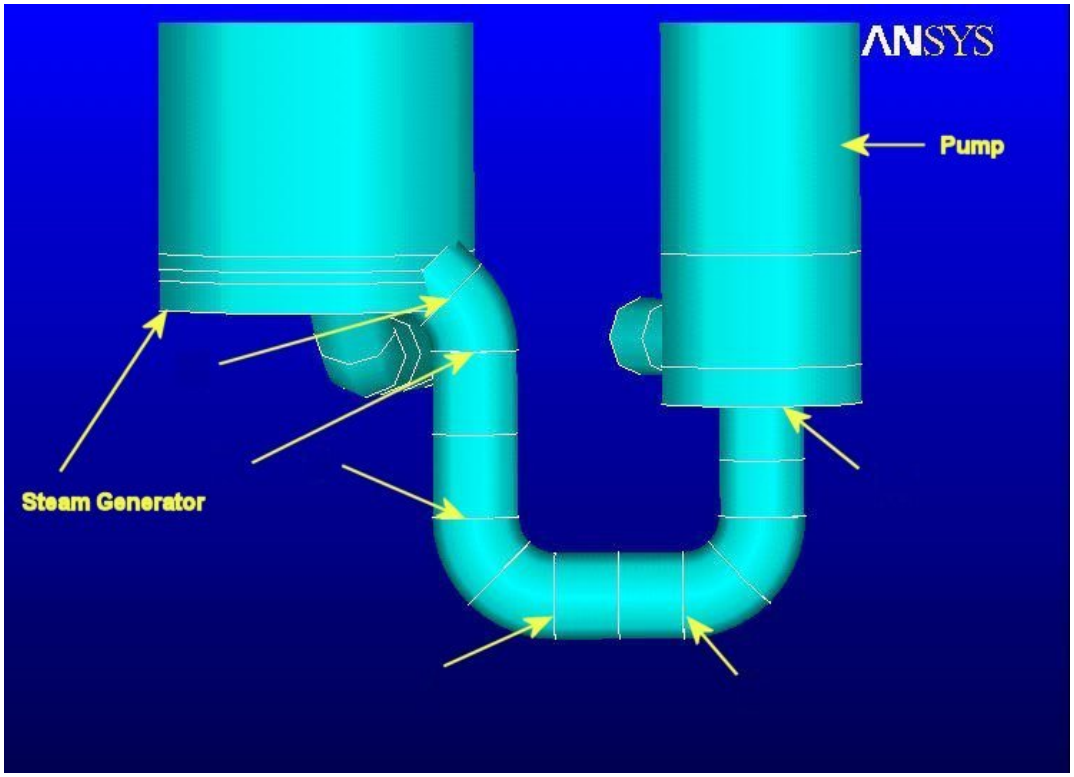

Figure C.45 PWR primary piping margin evaluation locations, 2 of 2

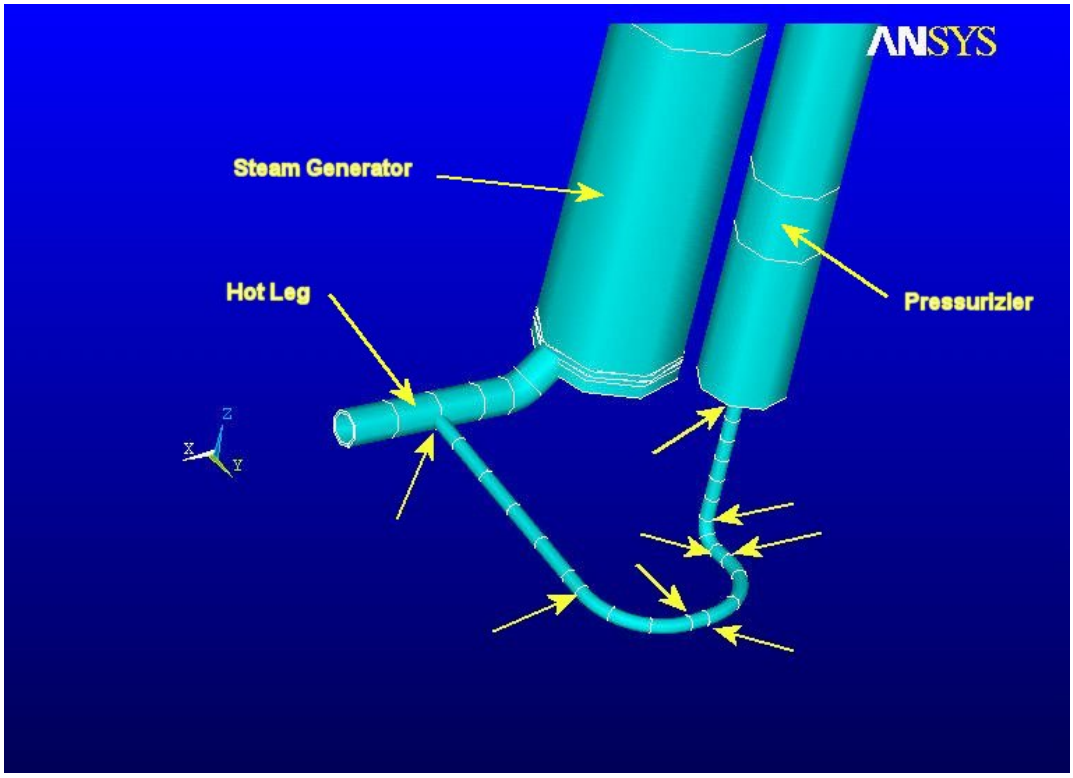

Figure C.46 PWR surge line margin evaluation locations

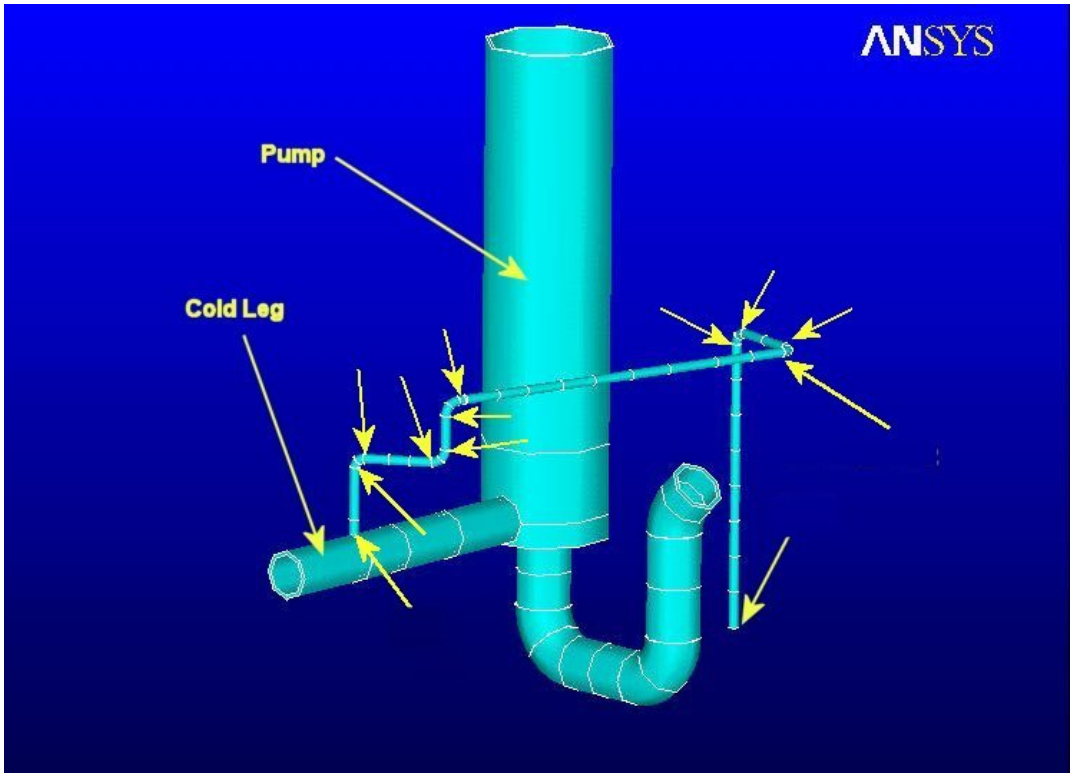

Figure C.47 Safety injection system line margin evaluation locations

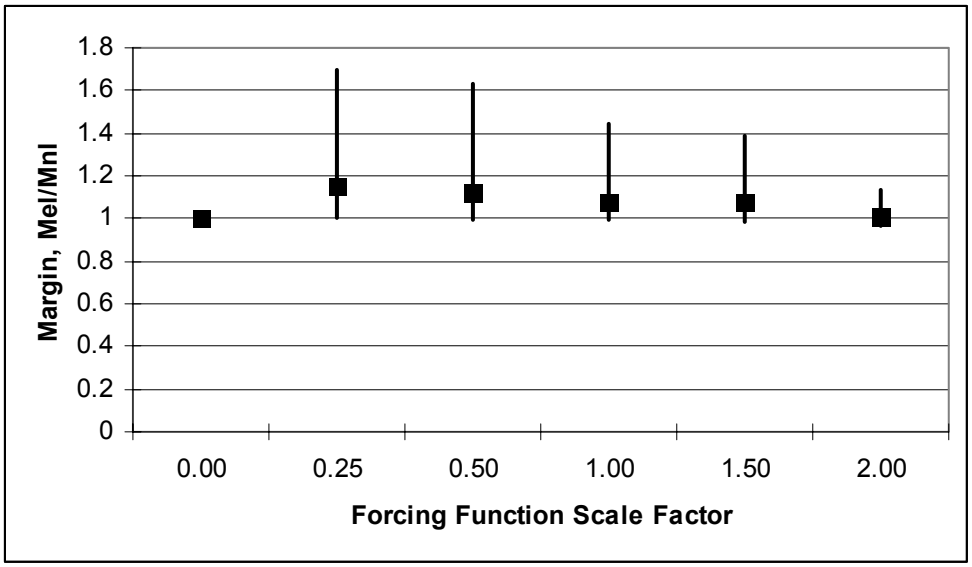

Figure C.48 Margins from the PWR hot leg locations

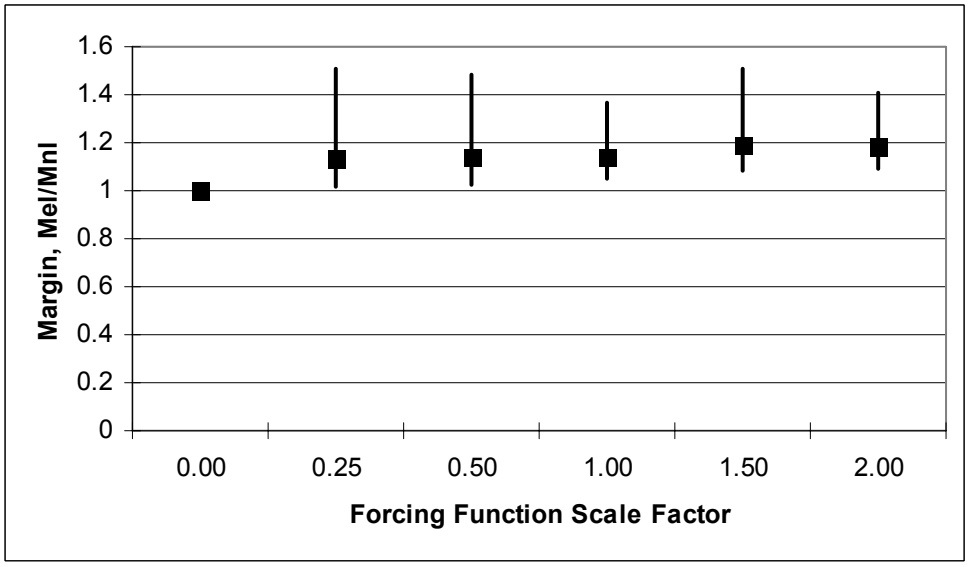

Figure C.49 Margins from the PWR cross-over leg locations

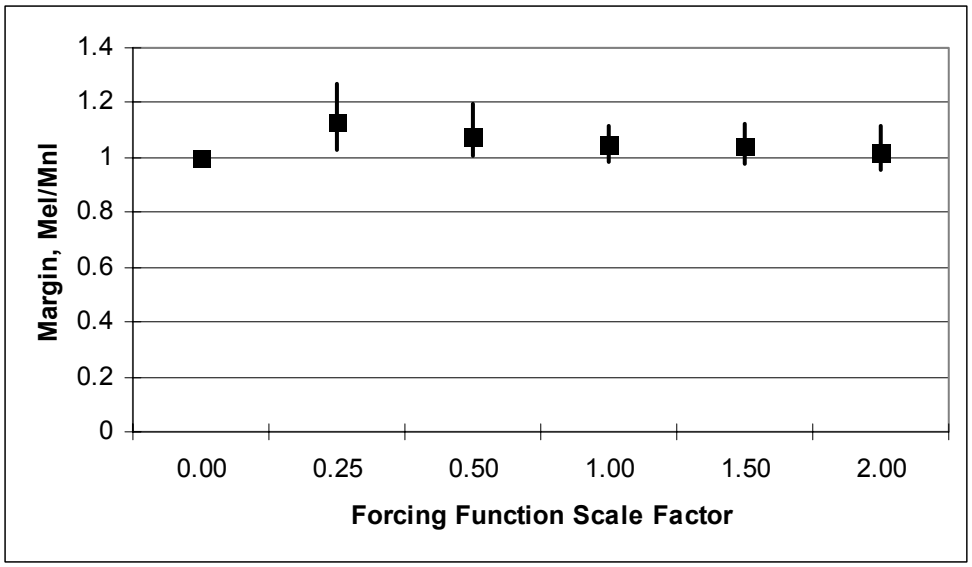

Figure C.50 Margins from the PWR cold leg locations

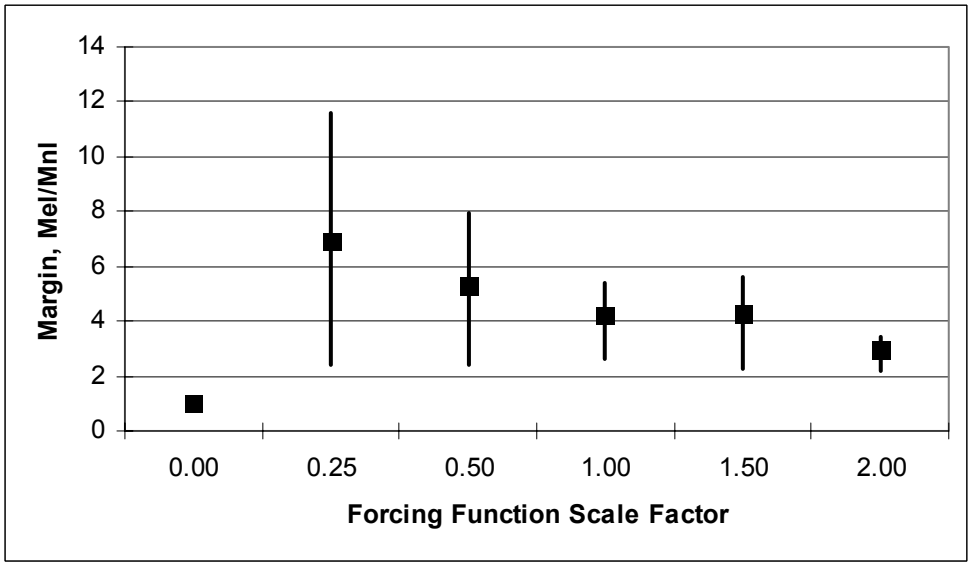

Figure C.51 Margins from the PWR surge line locations

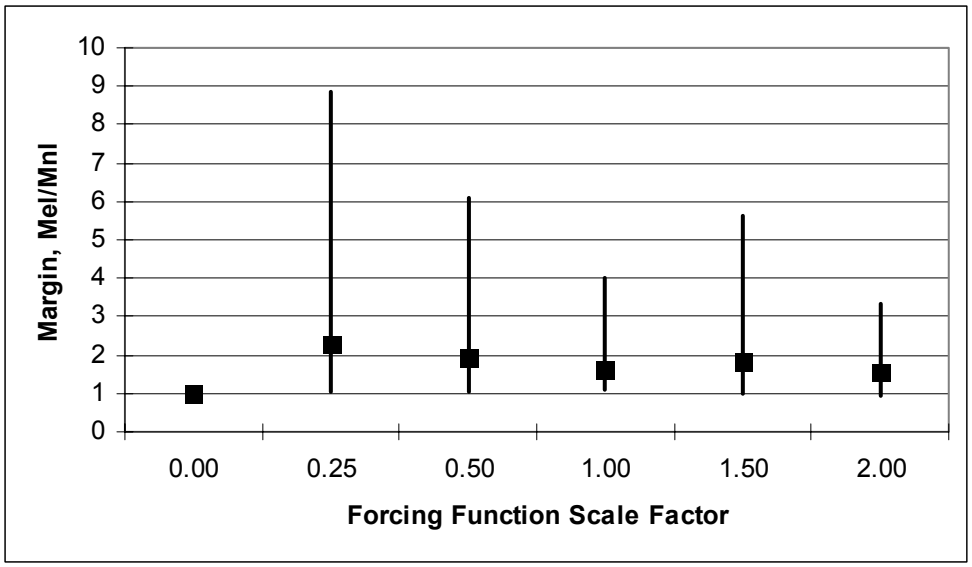

Figure C.52 Margins from the PWR safety injection system line locations

nonlinear and must be conducted in the time domain, they are significantly more expensive than the traditional linear analyses, because of the time stepping requirement, convergence issues, and inability to use superposition.

The IPIRG pipe system results from this task provide a tantalizing view of the potential to realize margin in plant piping. From a practical perspective, it is probably fortunate that the Actual Margins task was not conducted experimentally—very little could have been learned from one or two IPIRG pipe system experiments.

It must be recognized that, within the constraints of what was done in this task, it is not possible to categorically state that margin always exists in all plant piping. Only one seismic signature was applied from a single direction, only a normal operating condition was considered, flaws were not introduced into the piping, and the finite element model may have shortcomings. What can be stated, however, is: 1) That well-developed tools exist to conduct analyses that can determine if margin really exists, and 2) There is a distinct possibility that significant margin can be found, if the effort to conduct the required analyses can be justified.

C.5 References

C.1 Scott, P., Olson, R., and Wilkowski, G., "The IPIRG-1 Pipe System Fracture Tests: Analytical Results," PVP Vol 280, pp 153-163, June 1994.

C.2 Olson, R., Wolterman, R., and Wilkowski, G., "Margins from Dynamic FEM Analysis of Cracked Pipe Under Seismic Loading for the DOE New Production Reactor," PVP Vol 280, pp 119-134, June 1994.

C.3 Poole, A., Battiste, R., and Clinard, J., "Pipe Break Testing of Primary Loop Piping Similar to Department of Energy's New Production Reactor-Heavy Water Reactor," Oak Ridge National Laboratory, ORNL/NPR-92/64.

C.4 Scott, P. and others, "IPIRG-2 Task1 – Pipe System Experiments with Circumferential Cracks in Straight-Pipe Locations," NUREG/CR-6389, February 1997.

C.5 Olson, R., Wolterman, R., and Wilkowski, and G., Kot, C., "Validation of Analysis Methods for Assessing Flawed Piping Subjected to Dynamic Loading," NUREG/CR-6234, August 1994.

C.6 Hutchinson, J.W., "Plastic Buckling," *Advances in Applied Mechanics* (C.Yin, ed.) Academic Press, New York, 1974, pp. 67-144.

C.7 Scott, P., and others, "Crack Stability in a Representative Piping System Under Combined Inertial and Seismic/Dynamic Displacement-Controlled Stresses – Subtask 1.3 Final Report," NUREG/CR-6233 Vol. 3, June 1997.

C.8 Scott, P., Olson, R., and Marschall, C., "Data Record Book 1.2.8.3 for IPIRG Experiment 1.3-3," Report to US NRC, August 1990.

C.9 Rudland, D.L, Brust, F.W., and Wilkowski, G.M., "Fracture Toughness Evaluations of TP304 Stainless Steel Pipes," NUREG/CR-6446, January 1997.

C.10 Wilkowski, G. M., and others, "Short Cracks in Piping and Piping Welds" Seventh Program Report, March 1993 – December 1994, NUREG/CR-4599, Vol. 4, No., 1, April 1995.

C.11 Krishnaswamy, P., and others, "Fracture Behavior of Short Circumferentially Surface-Cracked Pipe," NUREG/CR-6298, November 1995.

C.12 Paul, D.D., and others, "Evaluation and Refinement of Leak-Rate Estimation Models," NUREG/CR-5128, Rev. 1, June 1994.

C.13 http://www.nucleartourist.com

C.14 http://www.nrc.gov (Note: much of the plant-specific content has been removed from the NRC's web site in light of the events of September 11, 2001)

C.15 Nero, A. V., "A Guidebook to Nuclear Reactors," University of California Press, Berkely CA, 1979.

C.16 Beaver Valley FSAR

C.17 http://www.sassi2000.com

C.18 Richart, F.E, Woods, R.D, and Hall, J.R., *Vibration of Soils and Foundations*, Prentice-Hall, Englewood Cliffs NJ, 1970.

C.19 American Society of Civil Engineers, *Seismic Analysis of Safety-Related Nuclear Structures and Commentary on Standard for Seismic Analysis of Safety Related Nuclear Structures*, ASCE 4-86, ASCE, New York, 1987.

C.20 Luco, J.E., and others, "Engineering Characterization of Ground Motion – Task II: Soil Structure Interaction Effects on Structural Response," NUREG/CR-3805 Vol. 4, August 1986.

C.21 Kennedy, R.P., "Engineering Characterization of Ground Motion – Task II: Effects of Ground Motion Characteristic on Structural Response Considering Localized Structural Nonlinearities and Soil-Structure Interaction Effects," NUREG/CR-3805 Vol. 1, March 1985.

C.22 Shao, L.C., "Summary of Frequencies for Reactor and Auxiliary Buildings," USNRC Private Communication, March 1975.

C.23 http://nisee.berkeley.edu/data/strong_motion/sacsteel/ground_motions.html

C.24 http://nisee.berkeley.edu/data/strong_motion/sac steel/motions/bo2in50yr.html